Sedimentary facies characterization through CPTU profiles: An effective tool for subsurface investigation of modern alluvial and coastal plains

BRUNO CAMPO* (iD), LUIGI BRUNO† (iD) and ALESSANDRO AMOROSI* (iD)
*Dipartimento di Scienze Biologiche, Geologiche ed Ambientali (BiGeA), Università degli Studi di Bologna, Piazza di Porta San Donato 1, 40126, Bologna, Italy (E-mail: bruno.campo@unibo.it)
†Dipartimento di Scienze Chimiche e Geologiche, Università degli Studi di Modena e Reggio Emilia, Via Giuseppe Campi 103, 41125, Modena, Italy

ABSTRACT

Cone penetration tests, a method that is typically used to determine the engineering properties of soils, can be used as an effective tool for refined subsurface stratigraphic investigations of alluvial and coastal plains, aside from the geographic location. High-resolution calibration of piezocone penetration tests (CPTU) with 20 sediment cores enabled the detailed characterization of alluvial, deltaic and coastal depositional systems of the Po Plain. Twelve cored facies associations, typical of alluvial and coastal plain environments, were characterized based on four distinct CPTU profiles: basic cone resistance (Q_c), sleeve friction (F_s), water pore pressure (U) and friction ratio (FR). Sandy facies associations (fluvial/distributary channel, bay-head delta, transgressive barrier, delta-front/beach-ridge) typically have high (>4 MPa) Q_c, low-to-negative U and low (<2%) FR. Muddy deposits (well-drained/poorly-drained floodplain, swamp, lagoon and prodelta) exhibit opposite trends. Heterolithic facies associations (crevasse-levée, offshore/delta-front transition) display characteristic seesaw profiles. Plotting of late Quaternary deposits onto the latest version of the cone penetration test typical soil behaviour chart (Robertson, 2010) enables the identification of distinctive facies associations reflecting distinctive grain size. CPTU interpretation leads to sedimentary facies recognition well beyond the simple lithological differentiation and, in particular, allows the refined characterization of clay-rich and silt-rich depositional units (swamp clays and peats, central-inner and outer lagoon, proximal/distal prodelta deposits) that exhibit only subtle differences in lithology. CPTU data can also serve for the accurate detection of key stratigraphic surfaces with potential engineering applications, such as the Pleistocene–Holocene boundary. This latter, a common feature of several alluvial and coastal plain successions, is commonly marked by an abrupt upward decrease of basic cone resistance and sleeve friction from Late Pleistocene, pedogenized, stiff strata to overlying Holocene, organic-rich, soft deposits. This study offers an updated CPTU-facies characterization method that could be suitable for subsurface investigations of modern alluvial and coastal plains worldwide.

Keywords Alluvial and coastal plains, CPTU, *in situ* facies characterization, Late Quaternary strata, Po Basin, stratigraphic profiling.

INTRODUCTION

Cone penetration (CPT) and piezocone tests (CPTU) have been utilized originally for geotechnical and engineering purposes, such as soil characterization and site assessment (Robertson *et al.*, 1986; Lunne *et al.*, 1997; Rampello & Callisto, 1998; Schneider *et al.*, 2008; Lo Presti *et al.*, 2009; Long & Donohue, 2010; Lorenzo *et al.*, 2014). Different studies showed their valuable potential for sedimentological analysis and subsurface stratigraphic investigations of unconsolidated, non-gravel deposits of modern coastal and delta plains worldwide (Schoustra, 1975; Taylor *et al.*, 1993; Devincenzi *et al.*, 2003; Lafuerza *et al.*, 2005; Sarti *et al.*, 2012; Zhang *et al.*, 2018; Helfensdorfer *et al.*, 2020). CPT–CPTU have also been utilized for subsurface reconstructions (Coerts, 1996; Törnqvist *et al.*, 2000; Hijma *et al.*, 2009; Amorosi *et al.*, 2020), geoarchaeological surveys (Bates *et al.*, 2007; Vos *et al.*, 2015; Koster, 2016), groundwater remediation (Quinnan *et al.*, 2010), hydrostratigraphic characterization (Campo *et al.*, 2020a), hydrogeological investigation (Stegmann *et al.*, 2011; Gu *et al.*, 2021) aquifer modelling (Flach *et al.*, 2005; Gueting *et al.*, 2015) and estimation of liquefaction hazard (Facciorusso *et al.*, 2015; Romeo *et al.*, 2015).

Identification of soil type has been one of the primary applications of CPT (Robertson, 2010). Soil texture classification has been generally accomplished by utilizing charts that link CPT parameters (i.e. the resistance to penetration at the tip of the penetrometer or cone resistance Qc, the friction of the sediment along the sleeve of the tool or sleeve friction Fs, and their ratio or friction ratio FR) to soil type (Begemann, 1965; Schmertmann, 1969). CPTU additionally provides water pressure (U), which is particularly useful for sand detection (Missiaen *et al.*, 2015). Following calibration with sediment core analysis from the same sites, CPT–CPTU may offer continuous (*in situ*) views of sedimentological data with great accuracy, repeatability and economical convenience for facies identification (Schokker & Koster, 2004; Truong *et al.*, 2016), stratigraphic correlation (Moran *et al.*, 1989; Beets *et al.*, 1996; Curzi *et al.*, 2017), mapping (Powell & Quarterman, 1995) and sequence stratigraphic interpretation (Styllas, 2014; Zhang *et al.*, 2014). However, despite this relatively large body of research, little attention has been dedicated to sedimentary facies characterization through CPT–CPTU profiles, and very few studies have clearly documented CPT–CPTU signatures of 'facies' (Lafuerza

et al., 2005; Choi & Kim, 2006; Amorosi *et al.*, 2017a; Zhang *et al.*, 2018; Bruno *et al.*, 2019).

In Canada, Monahan (1999) showed that deltaic sedimentary 'facies' have distinct signatures on CPT data. In The Netherlands, Schokker & Koster (2004) identified seven 'facies units' and used CPT to improve the characterization of Pleistocene aeolian and fluvial deposits and to correlate stratigraphic data. In the Llobregat delta plain (Spain), using Qc and FR parameters, Lafuerza *et al.* (2005) characterized six 'sediment facies' within a delta depositional system. In the macrotidal setting of the Qiantang River estuary (China), Zhang *et al.* (2018) distinguished five facies associations by CPT profiles.

In the southern Po Plain (Italy), after the pioneering work of Amorosi & Marchi (1999), who tested a CPTU-based method for facies characterization, several studies used CPTU parameters to improve subsurface stratigraphic analysis. Amorosi *et al.* (2017a) focused on alluvial facies and, in particular, on palaeosol recognition through CPTU profiles. Bruno *et al.* (2019) characterized estuarine and delta plain facies associations, with a focus on peat-layer detection and mapping.

However, none of these studies has provided a comprehensive documentation of the wide range of post-Last Glacial Maximum (LGM) facies associations, from proximal to distal depositional systems, in terms of CPT/CPTU basic parameters (i.e. non-normalized Qc, Fs and their ratio FR) plus U (for CPTU only), and a thorough analysis of their engineering properties is still lacking in the worldwide literature. Mud-dominated facies within alluvial and coastal plain regions are especially poorly known and their sedimentological–geotechnical characterization is still lacking. This work aims at filling this gap.

Based on the simultaneous interpretation of all of the above-mentioned parameters, a robust methodology for facies identification is proposed besides the soil charts, because no single parameter is diagnostic of a specific facies association, but their assemblage is (Amorosi & Marchi, 1999). The use of basic parameters makes this method independent from information that typically is not available during drilling operations (soil unit weight, groundwater conditions, etc.). This aspect may be of particular interest for geotechnical engineers that are generally interested in the *in situ* soil behaviour (Robertson, 2010) and, more in general, to geologists during exploration campaigns in alluvial and coastal plain settings all over the world.

Through calibration of CPTUs with detailed stratigraphy from 20 continuous cores from the

subsurface of the modern Po alluvial and delta plains (Fig. 1), and the integration of palaeontological and sedimentological data from previous studies, the specific objective of this study is to test the CPT/CPTU-based method for facies identification and characterization as an independent, fast, simple and economical stratigraphic tool.

GEOLOGICAL SETTING

The Po Plain (Fig. 1A) is one of the largest alluvial plains in Europe and the most densely populated area in Italy. It is drained by the Po River (652 km) and by its Alpine and Apenninic tributaries (Fig. 1A). The study site, covering an area
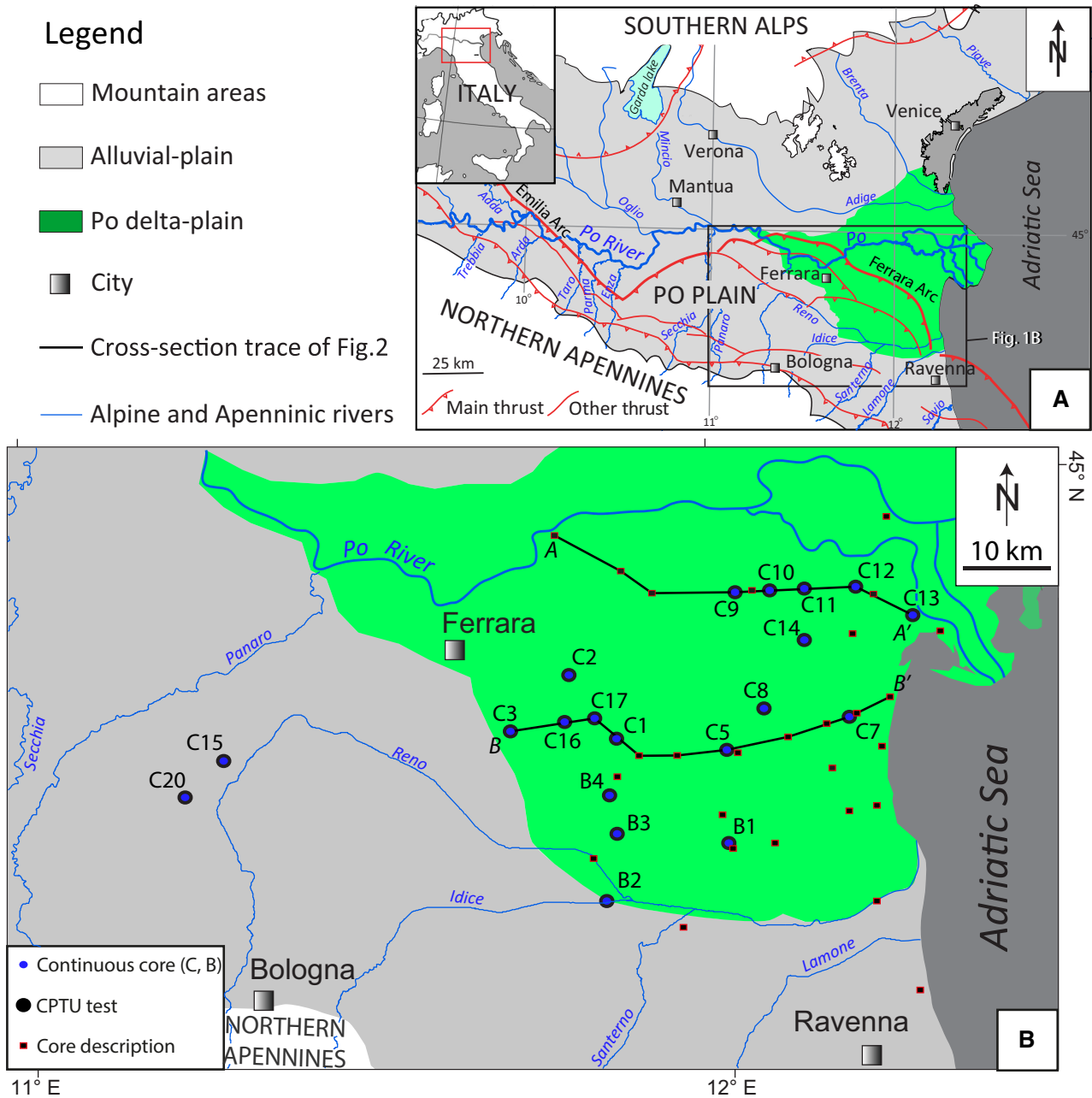

Fig. 1. (A) Geological map of the Po Plain (modified after Bruno *et al.*, 2019), with indication of the main buried structures (modified after Burrato *et al.*, 2003) and rivers. The study area is marked by the black rectangle. (B) Location of the study area with positions of the geological tests mentioned in this paper and section traces of Fig. 2. The modern Po delta plain is highlighted in green, whereas mountain chains, the Southern Alps and the Northern Apennines, are in white.

of *ca* 3000 km², largely corresponds to the modern delta plain (Fig. 1B).

The Po Plain is part of the rapidly-subsiding Po Basin that formed in response to the convergence between Africa and Eurasia since the Cretaceous (Carminati & Doglioni, 2012), leading to the formation of two orogens with opposite vergence: the southern Alps and the northern Apennines (Fig. 1A). These two mountain chains delimit the Po Basin to the north and to the south, respectively (Fig. 1A). South-Alpine buried structures consist of a single arc-shaped thrust system running from west to east, close to the Garda Lake (Vannoli *et al.*, 2015). Northern Apennines buried structures include the Emilia arc to the west and the Ferrara arc to the east (Fig. 1A). These thrust systems became active in the Late Miocene (Boccaletti *et al.*, 2011) and are considered to be still active.

The sedimentary infill of the Po Basin is characterized by a general shallowing-upward trend of Pliocene deep-marine to Quaternary shallow-marine and continental deposits (Ori, 1993). The Pliocene–Quaternary succession is up to 8 km thick in the main depocentres (Pieri & Groppi, 1981). Beneath the study area (Fig. 1), Middle Pleistocene–Holocene strata, *ca* 70 m thick, are composed of alluvial deposits, which accumulated under sea-level fall and lowstand conditions during glacial periods, alternating with coastal to shallow-marine sediments deposited during the ensuing post-glacial transgressions and interglacial highstands (Amorosi *et al.*, 2004). The uppermost coastal to shallow-marine interval is dated to the Holocene (Amorosi *et al.*, 2017b). The Holocene succession of the Po Plain exhibits a maximum thickness of about 30 m and a large variety of sedimentary facies (Bruno *et al.*, 2017; Campo *et al.*, 2017). Sand bodies consist of bay-head delta, distributary-channel, transgressive-barrier, beach-ridge and delta-front facies; the muddy units are characterized by soft, paralic and shallow-marine deposits (Fig. 2A and B). The Holocene deposits unconformably overlie Late Pleistocene alluvial units, composed of coarse-grained, (fluvial-channel, crevasse/levée) and fine-grained (floodplain; Fig. 2A and B) facies associations. The boundary between Late Pleistocene and Holocene strata is represented by a weakly-developed palaeosol (Fig. 2A and B) across a wide sector of the southern Po Plain (Bruno *et al.*, 2022). The study units are invariably finer-grained than gravel size, which favours the application of the CPTU method. The groundwater level fluctuates from 1 to 4 m depth throughout the study area.

The Holocene succession has been subdivided into eight millennial-scale parasequences (Fig. 2A and B; Amorosi *et al.*, 2017b). Early Holocene estuarine deposits form parasequences 1 to 3 that are stacked into a retrogradational pattern (Fig. 2A and B) reflecting the stepwise post-glacial sea-level rise (Bruno *et al.*, 2017). Aggradationally to progradationally-stacked parasequences 4 to 8 (Middle–Late Holocene; Fig. 2A and B) record the multi-phase Po delta upbuilding, with activation/deactivation of distributary-channels and delta lobe switching (Amorosi *et al.*, 2019).

METHODS

Twenty continuous cores, 20 to 36 m long, were recovered in close proximity (<20 m) to pre-existing CPTU tests (30–35 m deep; Fig. 1), during two drilling campaigns, in 2013 to 2015 and 2016 to 2018.

Average sediment recovery was >90%. Cores were analysed for sedimentology (lithology, grain-size trends, sedimentary structures, upper and lower boundaries, thickness, colour, and accessory materials) and geotechnical properties, such as pocket penetrometer measurements on fine-grained sediments. Pocket penetrometers are accessible tools generally used for valuating consistency of soils and approximating their unconfined compressive strength during coring operations (Amorosi *et al.*, 2015). Palaeontological data and 114 ¹⁴C dates, available in Amorosi *et al.* (2017a,b, 2019) and Bruno *et al.* (2017), were considered.

The CPTU profiles used in this work are part of the subsurface database of the Emilia-Romagna Geological, Seismic and Soil Survey, freely accessible online at https://applicazioni.regione.emilia-romagna.it/cartografia_sgss/user/viewer.jsp?service=geologia.

A commercial standard piezocone device was adopted in conformity to the international standard (ISSMFE, 1989) and reference test procedures (ISOPT, 1988). The test equipment is made of a 60° cone, with a 10 cm² base area and a 150 cm² friction sleeve positioned above the cone. Cells used to measure Qc and Fs values are included within the system. The filter for pore pressure is located behind the cone tip. An average speed of about 2 cm/s was selected to realize CPTs. A hydraulic jacking and reaction system mounted on a heavy truck with screw anchors form the pushing equipment, with thrust capacity of 20 tonnes.
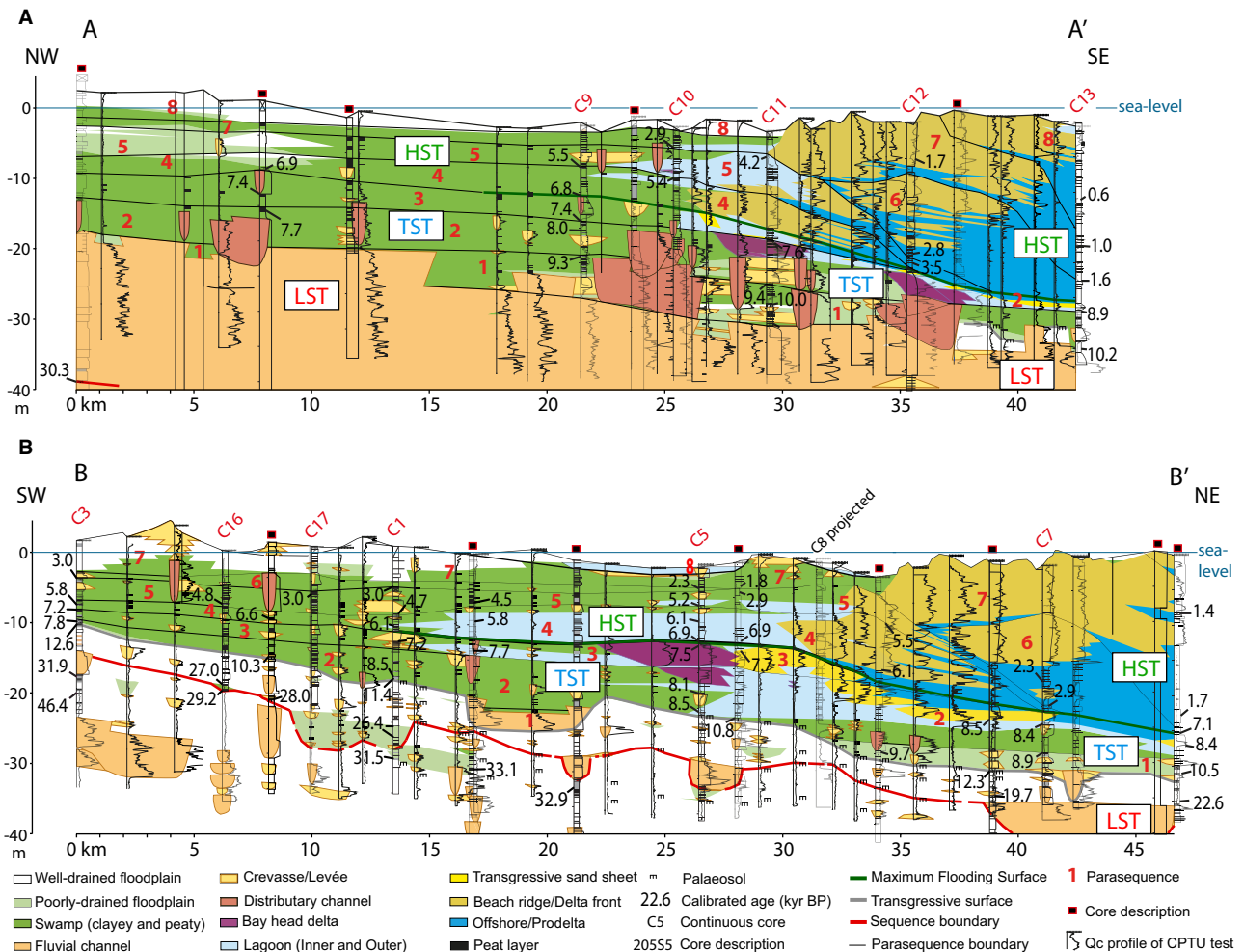
Fig. 2. Stratigraphic cross-sections showing the Late Pleistocene–Holocene stratigraphic architecture of the Po coastal plain (modified after Amorosi *et al.*, 2017b; Fig. 1B for location): (A) A–A' cross-section; (B) B–B' cross-section. Qc, Cone tip resistance; LST, lowstand systems tract; TST, transgressive systems tract; HST, highstand systems tract.

The results of CPTU tests are depicted through four curves (Fig. 3). Three profiles represent the vertical variations of the following parameters: Qc (non-normalized cone tip resistance), Fs (sleeve friction) and U (pore water pressure). The fourth curve represents the friction ratio (FR = fs/Qc × 100), which is used for the evaluation of sediment type in the most common soil-charts (Robertson, 2010). As also documented by Devincenzi *et al.* (2004), the use of Qc is due to several reasons: (i) Qc ability to distinguish between sedimentary facies with contrasting mechanical response; (ii) the fact that the distinction between non-normalized and normalized tip resistance does not bring more accuracy, especially for soft facies distinction; and (iii) the possibility of also including CPT tests, as Qc is a common

parameter for both. These latter are generally even more common than CPTUs in geological databases worldwide (Koster *et al.*, 2018). Furthermore, normalized charts require the detailed knowledge of parameters that are difficult to estimate and do not provide practical benefits when used at depth <30 m (Robertson, 1990) which corresponds to the maximum depth of the investigated succession.

Geotechnical characterization of individual facies associations was based on sedimentological criteria, following facies analysis on cores. All CPTU parameters were simultaneously examined and compared with the corresponding core segment.

The Robertson *et al.* (1986) chart is considered one of the most effective tools for sediment
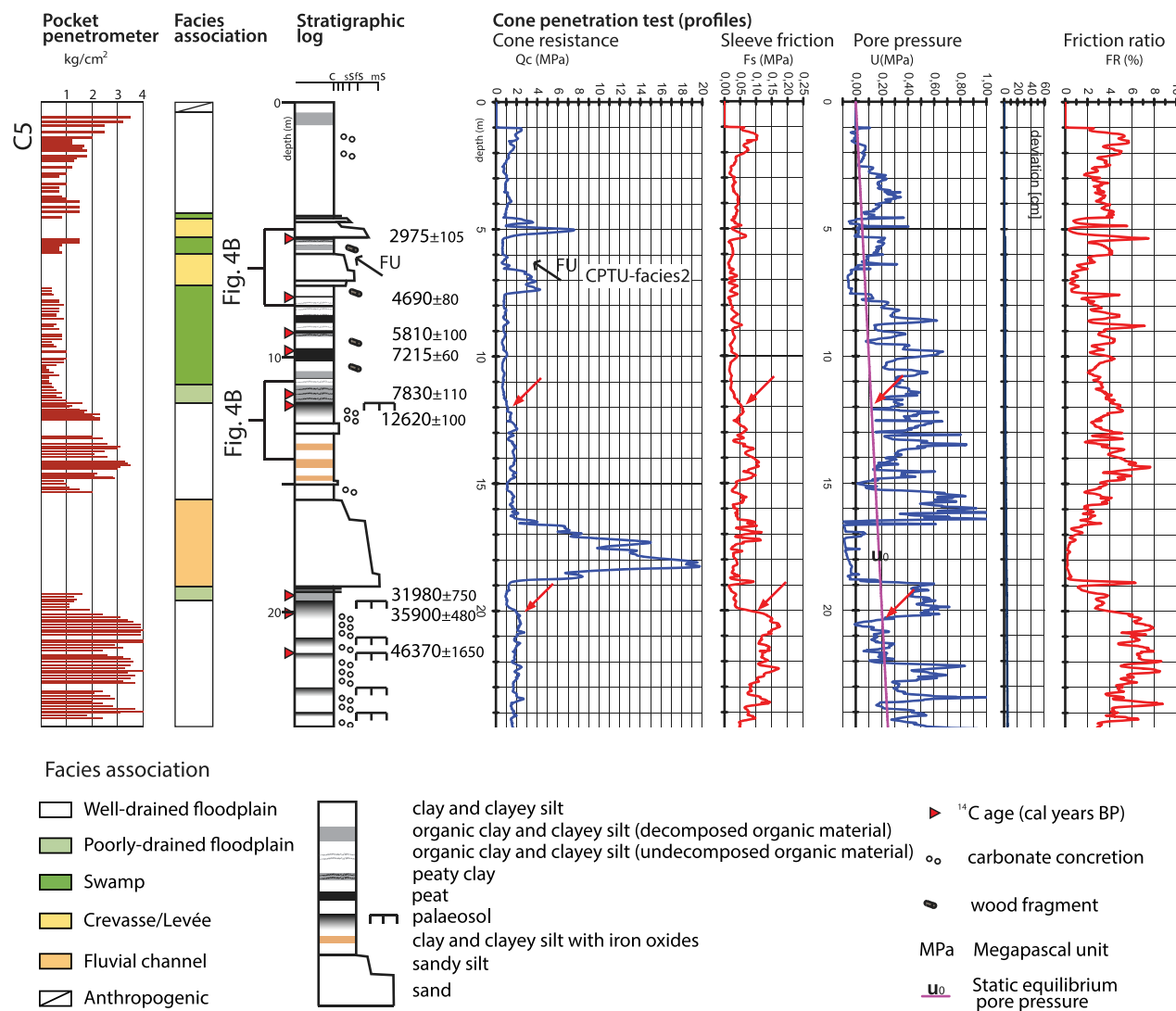
Fig. 3. Example of calibration between cone penetration test with piezocone (CPTU) and continuous core (C3, Fig. 1 for location). Pocket penetrometer measurements on fine-grained sediments provide an almost continuous record of *in situ* unconfined compressive strength that can be used for facies characterization (Amorosi *et al.*, 2015). Qc, Cone tip resistance; Fs, Sleeve friction; U, pore water pressure; u₀, static equilibrium pore pressure; FR, Friction Ratio; FU, fining-upward trend. Red arrows highlight the simultaneous increase in Qc and Fs, and the abrupt decrease in U of palaeosols.

classification (Berry *et al.*, 1998) and has become popular also among stratigraphers (Lafuerza *et al.*, 2005; Styllas, 2014; Zhang *et al.*, 2018; Helfensdorfer *et al.*, 2020). In this study, Qc was plotted against FR in the updated, non-normalized soil behaviour type (SBT) chart of Robertson (2010). In this latter, soil behaviour zones were reduced from 12 to 9 to match the normalized chart of Robertson (1990), and the dimensionless cone resistance (Qc/Pa) was plotted against FR, both on log scales to expand the portion where FR < 1%.

CPTU CHARACTERIZATION OF FACIES ASSOCIATIONS

In the alluvial and coastal sectors of the Po Basin, Late Pleistocene–Holocene facies associations have been broadly described based on their sedimentological and palaeontological characteristics and, where available, using pollen data (Bruno *et al.*, 2017; Campo *et al.*, 2017; Cacciari *et al.*, 2018; Amorosi *et al.*, 2021). In these works, geotechnical data have been considered as useful, but secondary, information to support sedimentological

interpretation (Amorosi *et al.*, 2015, 2017a; Bruno *et al.*, 2019). This study, instead, focuses on the CPTU characteristics of 12 facies associations that were grouped into four depositional systems. These are described below from proximal (alluvial) to distal (shallow-marine) settings.

An example of sediment core-CPTU test calibration is shown in Fig. 3. Depth correspondence between cores and CPTU curves is about 95%, with <1 m offset (Fig. 3). As documented by previous work (Schokker & Koster, 2004; Missiaen *et al.*, 2015), this is most likely caused by compression of soft deposits during core recovery (Koster, 2016). Distinctive sedimentological and CPTU characteristics are summarized in Table 1.

Alluvial plain deposits

This depositional system includes Late Pleistocene and Holocene facies associations (Figs 2 and 4).

Table 1. Summary diagnostic features of facies associations characterized in this paper.

	Sedimentological features, accessories and CPTU characteristics	Qc (MPa)	Fs (MPa)	U (MPa)	FR (%)
Fluvial-channel; (Fc)	Sharp base and top, FU trend*, >2 m thick	5–20 (>20)	0.05–0.1	<0 (negative)	<0.5
Crevasse/Levée; (Cr/Lv)	Gradational base and sharp top, CU trend* (splay); sharp base and top, FU trend*, <1.5 m thick (channel); silt-sand alternations, plant debris and rootlets (levée), <2 m thick, seesaw profiles	0.5–8.0 2.0–15.0 1.5–8.0	0.05–0.1 <0.05 0.05–0.12	$\leq u_0$, <0 $\leq u_0$, <0 >u_0, >0 (positive)	<2 0.5–1.0 2.0–8.0
Well-drained floodplain; (Fp)	Mottling, palaeosols, bioturbation, root traces, up to >10 m thick	1–10 (>20)	0.05–0.18	>>u_0, >0	3.5–10.0
Distributary-channel; (Dc)	Sharp base and top, FU trend*, <5 m thick	1–10 (>20)	<0.05	<u_0	<1
Bay-head delta; (Bhd)	Erosional or sharp base, sharp top, CU trend*, <5 m thick	5–20 (>20)	0.05–0.1	<u_0	<0.5
Swamp (Sw)	Wood fragments, plant debris, peat layers†	0.6–1.0	<0.02	0.05–0.75 >0 (>u_0)	1–6 (>10)
Poorly-drained floodplain; (Pdf)	Organic-matter-rich clay, carbonate nodules	0.8–1.8	0.025–0.1	>0	4–6 (10)
Lagoon; (Lg)	Bioturbation, subtle lamination, shell fragments; <3 m thick (inner: IL); bioturbation, silt/sand alternation, shell fragments; up to 5 m thick (outer: OL);	0.5–0.8 0.9–5.0	0.01–0.04 0.03–0.08	0.1–0.4 >0 (>u_0) 0.1–0.4 0 (>u_0, <u_0)	5–9 <4
Transgressive barrier; (Ts)	Erosional lower boundary, FU trend*, basal shell-rich lag; <2 m thick; CU trend*, gradational lower boundary (washover fan: Wf)	4–10 2–6	0.05 0.05	<u_0 <u_0	0.5–1.5 1–2
Beach-ridge/Delta-front; (Br/Df)	CU trend*, gradational lower boundary; 2.5–10 m thick	4–11 (>20)	<0.1	<u_0	<1
Offshore-Delta-front transition	Sand–clay alternation, plant debris, 1–3 m thick; seesaw profiles; (delta-front transition)	0.9–8.0	0.02–0.1	>0, <u_0	1–7
Offshore/Prodelta; (Of/Pd)	Bioturbated clay (offshore), <1 m thick; organic matter-rich silty clay to silt, up to 20 m thick, (proximal prodelta); organic matter-rich silty clay, up to 20 m thick, (distal prodelta)	0.6–1.0 0.3–0.6	0.025 0.01–0.025	0.3–0.75 (>u_0, <u_0) 0.2–0.3 (>u_0)	0.3–0.75 3–4

*Trend also in the Qc and Fs profiles. †Concomitant peaks in Qc, Fs, U and FR.
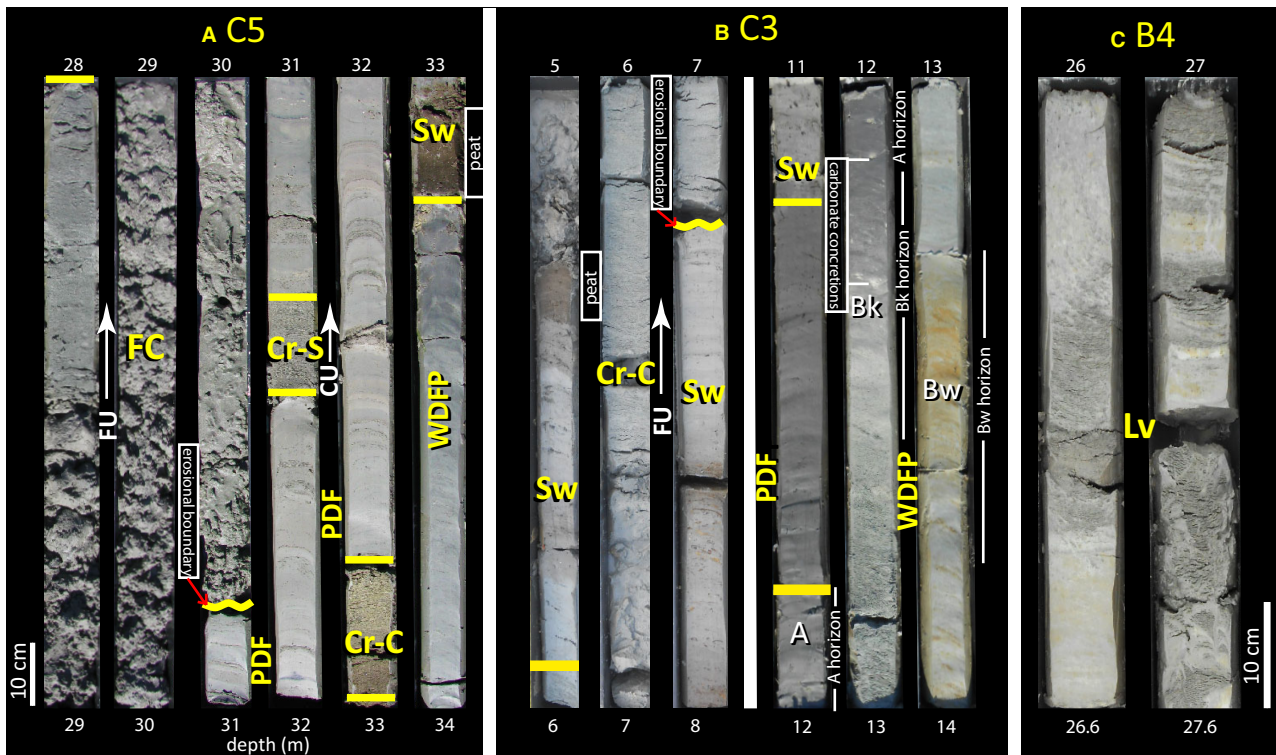
Fig. 4. Representative core photographs of alluvial, estuarine and deltaic facies associations. FC, Fluvial channel; Cr-C, Crevasse-channel; Cr-S, Crevasse-splay; Lv, Levée; WDFP, well-drained floodplain; A (white colour), A horizon of palaeosol; Bk, Bk horizon of palaeosol; Bw, Bw horizon of palaeosol; PDF, Poorly-drained floodplain; Sw, Swamp (Inner estuary and upper delta plain depositional system). (A) Core C5. (B) Core C3. (C) Core B4. FU, fining-upward trend; CU, coarsening-upward trend; Yellow line, boundary of facies associations; Wavy yellow line, erosional lower boundary.

Fluvial-channel facies association

Facies characteristics. This facies association is made of medium to coarse grey sands with erosional bases, fining-upward (FU) trends and sharp or transitional tops (Fig. 4A). Individual sand bodies, 2 to 10 m thick, can be vertically stacked to form multi-storey deposits (Fig. 2). High-angle, unidirectional cross-stratification and horizontal bedding are locally preserved. Macrofaunal remains are rare and generally represented by shell fragments. The meiofauna includes only sporadic fragments of freshwater ostracods.

Based on the combination of lithology, erosional lower boundary, thickness and fossil content, this facies association is interpreted as a fluvial-channel deposit. The FU tendency and presence of unidirectional flow structures strongly support this interpretation (Miall, 2013).

CPTU characteristics. This facies association is typified by high Qc values, in a range of 5 to 20 MPa, locally >20 MPa (Fig. 5A and Table 1). Fs is generally low (0.05 to 0.1 MPa), with very few exceptions (up to 0.2 MPa; Fig. 5). Water pore pressure (U) is commonly negative (<0) or lower than static equilibrium pore pressure u_0. Mean FR is <0.5%. The lower boundary is generally characterized by a sharp increase of Qc, followed upward by progressively decreasing values (Figs 3 and 5).

High Qc values and low FR percentages are consistent with coarse to medium fluvial sand deposits (Styllas, 2014). Low to negative U indicates high permeability and tendency to dilate (Moran *et al.*, 1989; Dafalla *et al.*, 2020). Peaks in Qc at lower boundaries and upward decreasing values are consistent with erosional bases and FU grain-size trends, both characteristic of fluvial-channel deposits.

Crevasse/levée facies association

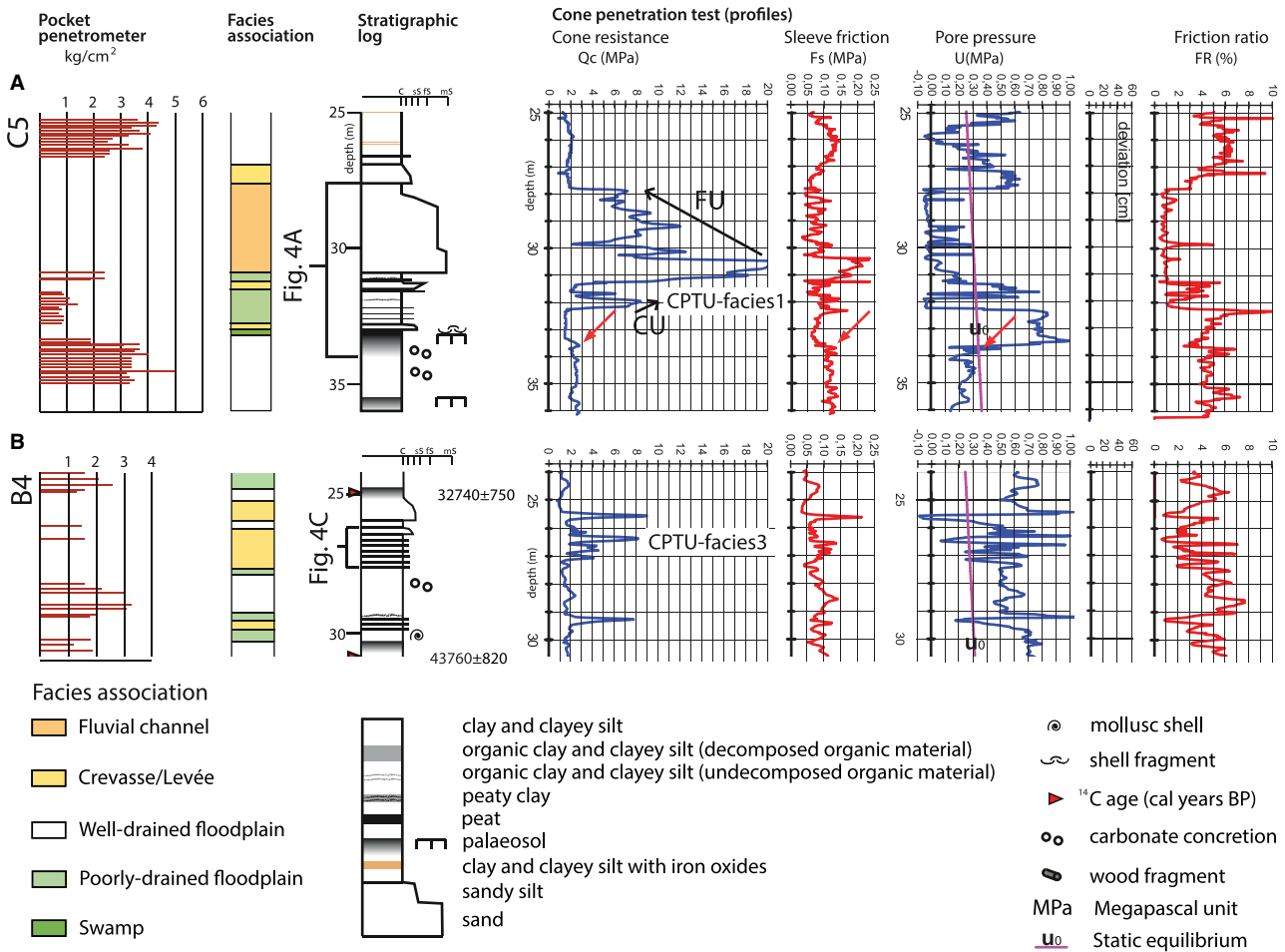*Facies characteristics.* This facies association includes three different lithofacies: lithofacies 1

Fig. 5. Identification of alluvial plain facies associations in different CPTU profiles (Qc, Fs, U and FR) and adjacent cores C5 (A) and B4 (B; Fig. 1 for location). FU, fining-upward trend; CU, coarsening-upward trend. Red arrows highlight the simultaneous increase in Qc and Fs, and the abrupt decrease in U of paleosols.

is characterized by coarsening-upward (CU) trends from grey clayey silts to silty sands, with gradational lower boundaries and sharp tops (Figs 4A and 6). Lithofacies 2 shows many similarities with fluvial-channel sand bodies (FU trend, erosional base and gradational top) but a typically lower thickness (<1.5 m) and finer grain size (medium to silty sands; Fig. 4B). Lithofacies 3 includes the repetitive alternation of grey to vari-coloured silty sand and silty clay (Fig. 4C). Plant debris and rootlets are locally abundant. Thickness is generally <2 m.

This facies association reflects deposition in three distinct sub-environments close to river channels (Bridge, 1984). Given its CU trend, gradational lower boundary and sharp top, lithofacies 1 is interpreted as a crevasse splay deposit. Lithofacies 2 represents a crevasse channel deposit, based on grain-size, thickness and FU

trend. The silty sand-silty clay alternations that typify lithofacies 3 most likely reflect traction plus fallout deposition. These lithological characteristics, along with indicators of subaerial exposure (plant debris and rootlets) are typical of natural levées.

CPTU characteristics. This facies association is characterized by peculiar values of CPTU parameters that allow the distinction of three CPTU-facies. In CPTU-facies 1 (Fig. 5A, *ca* 31.5–32.5 m CPTU-depth), Qc gradually increases upward, from 0.5 to 8 MPa. Fs ranges between 0.05 and 0.1 MPa. U is negative or <u₀. The FR curve mirrors the Qc profile, with percentages <2. CPTU-facies 2 (Fig. 3, *ca* 6.5–7.5 m CPTU-depth) shows low to negative U and decreasing upward trends of Qc and Fs, with generally lower values (2 < Qc < 15 and Fs < 0.05 MPa) than in fluvial-
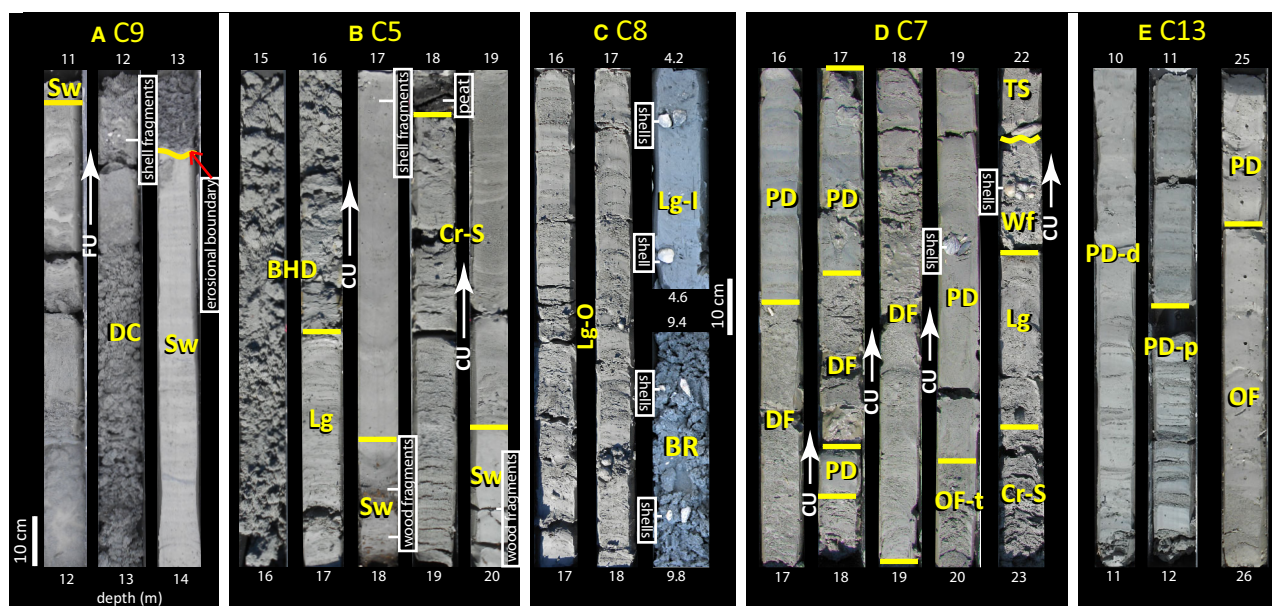
Fig. 6. Representative core photographs of estuary (inner and outer) and delta plain (upper and lower), nearshore and shallow-marine facies associations. BHD, bay head delta; Cr-S, Crevasse-splay; Lg, Lagoon (Inner: -I; Outer: -O); Sw, Swamp; DC, Distributary channel; TS, Transgressive sand sheet; Wf, Washover fan; BR, Beach ridge; DF, Delta front; OF, Offshore; OF-t, Offshore transition; PD, Prodelta (Proximal: -p; Distal: -d). (A): core C9; (B): core C5; (C): core C8; (D) core C7; (E): core C13. FU, fining-upward trend; CU, coarsening-upward trend; Yellow line, Lower and upper boundary of facies associations; Yellow-wavy line: erosional lower boundary.

channel deposits. On the other hand, FR is slightly higher (0.5–1.0%; Fig. 3). CPTU-facies 3 displays characteristic seesaw profiles (Fig. 5B, 26–27 m CPTU-depth), with Qc fluctuations in a range of 1.5 to 8.0 MPa. Fs is invariably lower than 0.12 MPa. In general, U has positive values, $>u_0$, although it locally may drop below u_0 (Fig. 5B). FR ranges between 2% and 6%.

Highly variable Qc (up to 15 MPa), FR (0.5–2.0%) and U (negative-to-positive) values are consistent with texturally heterogeneous facies ranging from medium sand to clayey silts (Styllas, 2014). Qc and Fs trends in CPTU-facies 1 are consistent with characteristic CU trends of crevasse splay deposits. On the other hand, Qc and Fs trends of CPTU-facies 2 are consistent with FU tendencies observed in crevasse-channel deposits in cores. Seesaw profiles in CPTU-facies 3 likely reflect sand–mud centimetre-thick alternations typical of natural levée deposits.

Well-drained floodplain facies association
Facies characteristics. This facies association, up to >10 m thick, is composed of massive and bioturbated silts and clays, with carbonate nodules, scant plant fragments and root traces (Fig. 4A and B). Locally, faint horizontal

lamination is observed. Yellowish to brownish clay mottles of Fe and Mn oxides can be present (Fig. 4B). Dark organic-rich silty clay layers overlying light grey horizons with calcite nodules are common features in the Late Pleistocene succession (Fig. 4A and B). Sparse fragments of freshwater gastropods can be found, whereas the meiofauna is generally absent.

This facies association has been interpreted as deposited in a well-drained floodplain. Bioturbation, lithology, macrofossils and accessory materials reflect a low-energy freshwater depositional environment dominated by suspension fallout, with prolonged episodes of subaerial exposures, as demonstrated by oxidized and pedogenically modified horizons (Buol *et al.*, 2011). These latter have been interpreted as weakly-developed palaeosols (Inceptisols of Soil Survey Staff, 1999), each composed of an organic-rich, commonly dark, eluvial horizon (A), and an illuvial Bw or Bk horizon (Fig. 4B), typified by a higher content of secondary calcite. Whereas horizon Bw is generally characterized only by incipient weathering with colour ranging between greyish brown to yellowish brown, secondary calcite content is higher in the more whitish grey Bk. This horizon generally includes characteristic nodules

of carbonates, a few millimetres to centimetres thick (Fig. 4B).

CPTU characteristics. This facies association displays a relatively narrow range of Qc values (1.2–3.0 MPa; Figs 3, 5A, 5B and Table 1). Fs values are generally high, up to 0.18 MPa, and U >> 0. Friction Ratio ranges between 3.5% and 10% (Figs 3, 5A and 5B). Individual palaeosols are marked by the subtle, but consistent downward increase in Qc (up to 1.2 MPa) coupled with a sharp spike in Fs (up to 0.12 MPa) and commonly an abrupt decrease in U (Figs 3 and 5A).

Qc and FR values are interpreted to represent floodplain silt–clay sediments (Sarti *et al.*, 2012). The simultaneous increase in Qc and Fs and the abrupt decrease in U reflect response to penetration of over-consolidated, pedogenized muds.

Estuary and delta plain deposits

This depositional system includes facies associations that formed in freshwater to brackish environments. This group dominates the Holocene succession in the proximal and central sectors of the study area, whereas it occurs at distal locations in thin, transgressive parasequences (Fig. 2).

Distributary-channel facies association
Facies characteristics. This facies association shares several features with fluvial-channel deposits, including lithology, FU trend and erosional lower boundary (Fig. 6A). Differently, it displays lower thickness (<5 m) and width (<1400 m; Bruno *et al.*, 2017), and is finer-grained (silty fine sand; Fig. 6B). Fragments of freshwater to low-brackish gastropods have been observed (Fig. 6A). Wood fragments are rare. This facies association is in lateral transition to organic-matter-rich muds.

Lithology and FU trend reflect deposition in active channels. However, based on the finer grain-size and lower thickness than fluvial-channel deposits, palaeontological data and lateral transition to organic matter-rich muds, this facies association is inferred to reflect distributary-channel deposits (Bhattacharya, 2006).

CPTU characteristics. This facies association is characterized by relatively high Qc values (1–10 MPa), locally exceeding 20 MPa (Fig. 7A; Table 1). Fs is generally <0.05 MPa, U < u_0 and FR < 1% (Fig. 7A). At the base, Qc may sharply increase to 6 MPa, whereas at the transition to overlying muds it decreases gradually (Fig. 7A).

Relatively high Qc, low FR and negative U are typical of sand bodies. Comparatively lower values of Qc and Fs, and sedimentary features of encasing deposits permit discrimination of distributary-channel deposits from fluvial-channel sand bodies. Distributary-channel-related facies (i.e. crevasse and levée deposits) are not described, because their sedimentological and geotechnical characters are similar to their fluvial counterparts.

Bay-head delta facies association
Facies characteristics. This facies association is composed of medium to fine grey sand (Fig. 6B). Its base is either erosional or sharp, whereas its top commonly is a sharp surface. The thickness of this facies association is generally <5 m, and sand bodies display a CU trend (Fig. 6B). Wood fragments and vegetal remains are locally encountered at the top. Body fossils, though generally poorly preserved, exhibit a diagnostic mixture of brackish (*Cyprideis torosa* and *Cerastoderma glaucum*) and freshwater (*Ilyocypris*) species (Amorosi *et al.*, 2017b). This facies association typically occurs at the transition from inner estuary (freshwater) to outer estuary (brackish) environments (Fig. 2).

Based on lithology, palaeontological data, grain-size trends and stratigraphic position, this facies association is interpreted as bay-head delta mouth deposits. The co-existence of brackish fossils and freshwater ostracods, along with the typical CU trend, are consistent with progradation of sand bodies into an estuarine (brackish) environment (Dalrymple *et al.*, 1992; Schwarz *et al.*, 2011), occasionally subject to fluvial input (Hijma *et al.*, 2009).

CPTU characteristics. This facies association shows relatively high Qc (up to >20 MPa; Table 1) and Fs (0.05–0.1 MPa) values. U is <u_0 (Fig. 7B). Its lower boundary is marked by the sharp increase of Qc (up to 7 MPA, Fig. 7B), which generally increases upward.

High Qc, low FR and U < u_0 are consistent with a coarse to fine sandy texture (Amorosi & Marchi, 1999). Upward increasing Qc values suggest a general CU grain-size trend, whereas the sharp increase in Qc at the base is consistent with the sharp lower boundary of bay-head delta deposits observed in cores.

Freshwater swamp facies association
Facies characteristics. This facies association, up to 15 m thick (Fig. 2), is composed of very soft grey to dark-blackish clays (Fig. 6A and B). Rare
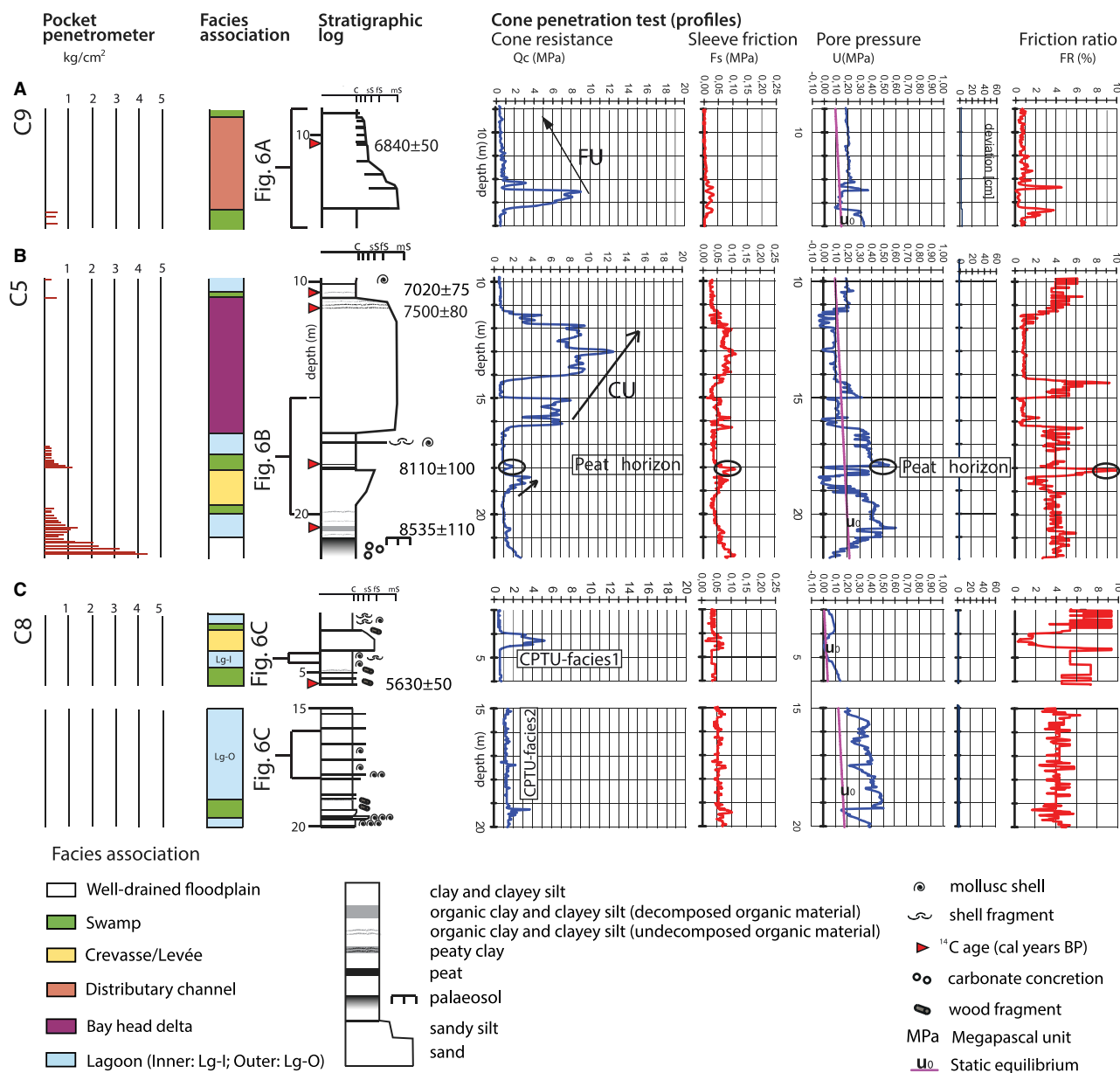
Fig. 7. Identification of estuary and delta plain facies associations in CPTU profiles (Qc, Fs, U and FR) and adjacent cores C9 (A), C5 (B) and C8 (C) (Fig. 1 for location). Black circles highlight peaks on CPTU that correspond to a discrete peat horizon. FU, fining-upward trend; CU, coarsening-upward trend. Lagoonal (inner: Lg-I; outer: Lg-O) facies associations identification in CPTU profiles (Qc, Fs, U and FR) and adjacent core (C8) (Fig. 1 for location).

silt to silty sand intercalations, at the centimetre-scale, are locally encountered. Wood fragments and vegetal remains are abundant at discrete horizons or scattered along decimetre-thick core segments (Fig. 6A and B). Iron and manganese oxides are absent. Peat layers, 10 to 40 cm thick, and mostly made of poorly decomposed wood fragments and plant remains, occur at different stratigraphic levels (Figs 4A, 4B and 6B).

Molluscs (*Bithynia tentaculate* and *Valvata macrostoma*) and freshwater ostracods (*Candona* and *Pseudocandona*) typify this facies association (Amorosi *et al.*, 2017b). Pollen data (Cacciari *et al.*, 2018) show that clayey intervals include open to dense alder carr vegetation, with a mixed oak–holm oak ecological component in subordinate position. On the other hand, peat layers are characterized by pollen grains of herbaceous

wetland community, with aquatic plants (hydrophytes), or sparse alder carrs, the latter being tolerant to prolonged intervals of radical drowning (helophytes).

Fine-grained and dark-coloured sediments with high organic-matter content and freshwater fossils suggest deposition in stagnant, semi-permanently flooded wetlands (for example, swamps; Salel *et al.*, 2016), as part of inner estuarine or upper delta plain environments. Peat layers likely accumulated under permanently waterlogged (high water table) and reducing conditions, as also demonstrated by the absence of traces of oxidation and presence of aquatic plants (Cacciari *et al.*, 2018). Conversely, grey clays were deposited under a relatively lower water table, close to an active channel, as suggested by rare coarser beds reflecting weak overbank deposition.

CPTU characteristics. This facies association is generally characterized by rectilinear Qc profiles, with values of 0.6–1.0 MPa (Fig. 6A and B). Fs is very low (<0.02 MPa), FR ranges between 1% and 6% and U is >0 (0.05–0.75 MPa), with linear increase with depth (Fig. 6). Peaks along the four CPTU profiles, recording a sharp increase in Qc (+1 MPa), Fs (+0.06 MPa), U (+0.15–0.45 MPa) and FR (up to 10%) coincide with the occurrence of peat horizons in core (circles in Fig. 6B).

Low Qc and Fs values and U > 0 are characteristic of fine-grained swamp deposits (Sarti *et al.*, 2012). Such values are significantly lower than those typically recorded in well-drained floodplain deposits. Distinctive peaks in Qc and Fs invariably associated with peat layers likely reflect post-burial peat consolidation (Bruno *et al.*, 2019).

Poorly-drained floodplain facies association
Facies characteristics. This facies association is composed of grey clays and silty clays. Carbonate nodules are sparse and less frequent than in well-drained floodplain deposits. Iron–manganese oxides are very rare and evidence of pedogenesis (for example, horizonation) is lacking. Plant fragments and organic matter are locally abundant but invariably in lower proportion than in swamp deposits (Fig. 4A and B). Shell fragments of freshwater molluscs (*Planorbia*) and freshwater to low-brackish ostracods (*Candona*) are found occasionally.

Lithology, the homogeneous grey colour, a lack of pedogenic features and the fossil content allow interpreting this facies association as accumulating in a low-energy setting, such as a poorly-drained floodplain, under the persistent influence of freshwater due to high water table or river floods (Bruno *et al.*, 2019).

CPTU characteristics. This facies association displays Qc values narrowly constrained between 0.8 to 1.8 MPa (Table 1). Fs is in a range of 0.03 to 0.1 MPa, U > 0 and FR 4 to 6% (up to 10%; Figs 3 and 5). Increasing values characterize this facies association from shallow (Qc *ca* 0.8 MPa, Fs *ca* 0.02) to relatively deeper stratigraphic intervals (Qc *ca* 1.8 MPa and Fs 0.07 MPa; Figs 3 and 5). In general, CPTU parameters from this facies association are transitional between well-drained floodplain muds and swamp clays.

Lagoon facies association
Facies characteristics. This facies association can be subdivided into two different lithofacies based on its lithological and sedimentological characteristics. Lithofacies 1, up to 3 m thick (Fig. 2), is made of soft homogeneous grey clay and silt (Fig. 6C). Bioturbation and subtle lamination are common and undecomposed organic matter is locally abundant. Shell fragments of brackish molluscs (*Cerastoderma glaucum*, *Abra segmentum*, *Loripes arbiculatus* and *Ecrobia ventrosa*) are widespread (Fig. 6C). The ostracod *Ciprideis torosa* and foraminifer *Ammonia tepida* are diagnostic species (Amorosi *et al.*, 2017b). This lithofacies is commonly transitional to swamp deposits. Lithofacies 2, up to 6 m thick (Fig. 2), consists of clay–sand alternations at the centimetre scale (Fig. 6C). Mollusc fragments (*Cerastoderma glaucum*, *Loripes arbiculatus* and *Lentidium Mediterraneum*) are abundant (Fig. 6C), whereas the meiofauna is characterized by *A. tepida*, *C. torosa*, *Leptocythere turbida* and *Miliolid species* (Amorosi *et al.*, 2017b). This lithofacies is in lateral transition to lithofacies 1 (landward) and to coastal sands (seaward, Fig. 2).

Sedimentological characteristics and the diagnostic fossil content are indicative of a brackish, semi-enclosed basin, such as a lagoon. Given its stratigraphic position, and the landward transition to freshwater, river-dominated deposits, this facies association could also be a part of a wider (outer) estuarine environment (Boyd *et al.*, 2006). The increasing sand/mud ratio from lithofacies 1 to lithofacies 2 reflects transition from low-energy (inner lagoon) to increasingly higher-energy (outer lagoon) sub-environments. This interpretation is supported by the highly diversified (brackish-marine) meiofauna content of lithofacies 2, compared to the oligotypic fossil association of lithofacies 1.

CPTU characteristics. In line with core data, this facies association shows two CPTU facies with distinct geotechnical characteristics. CPTU-facies 1 shares many characteristics with swamp deposits, such as very low Qc (0.5–0.8 MPa), Fs (0.01–0.04 MPa) and U > 0 (0.1–0.4 MPa; Fig. 7C). The Qc profile is rectilinear and FR is generally high (5–9%; Fig. 7C). CPTU-facies 2 is characterized by higher Qc values, fluctuating between 0.9 and 1.5 MPa, up to 5 MPa (Table 1), with seesaw-shaped profile (Fig. 8). Fs displays a similar profile, with values ranging between 0.03 and 0.08 MPa (Fig. 8). U is generally >0, but locally $<u_0$. Mean FR is <4% (Table 1).

Qc and FR in CPTU-facies 1 are consistent with a fine-grained, soft clay deposit. In CPTU-facies 2, seesaw profiles, with variable U, locally $<u_0$ values, reflect millimetre to centimetre-scale mud–sand alternations. Despite similar characteristics (seesaw profile and Qc values) between CPTU-facies 2 and the levée facies association, which makes their distinction quite difficult based on CPTU profiles alone, lagoon sediments are generally softer, as suggested by lower Fs measurements and FR percentages (see Table 1).

Nearshore sands

This depositional system consists of two sand-dominated facies associations that accumulated in nearshore environments, during the Holocene transgression and subsequent coastal progradation, respectively (Fig. 2).

Transgressive barrier facies association
Facies characteristics. This facies association is characterized by grey silty to fine sands with FU trend, erosional lower boundary and gradational top (Fig. 6D). Its thickness generally is <2 m, with mean values of about 1 m (Fig. 5D). The base is marked by a veneer of shell fragments of marine and brackish taxa (Fig. 6D). Above the erosional fossil-rich boundary, the meiofauna include only abraded specimens of *A. beccari*, *Elphidium Crispum* and *Pontocythere turbida* (Amorosi *et al.*, 2017b).

Below the shell lag, a silty to very fine sand body with characteristic CU trend is locally encountered (Fig. 5D). This sand body includes poorly-preserved euryhaline and shallow-marine taxa, such as *C. torosa*, *Ammonia* and *Elphidium* spp.

Based on the combination of lithology, sedimentological features, fossil content and thickness, this facies association is interpreted as deposited in a high-energy, coastal environment.

In particular, medium to fine sands with FU trend overlying the basal shell-rich lag are interpreted to represent transgressive barrier island deposits. The basal shell-rich lag reflects wave erosion and reworking of backshore and upper shoreface strata during barrier retreat (wave ravinement surface of Swift, 1968). The limited thickness suggests erosion of upper shoreface strata, probably cannibalized during shoreface retreat (Storms *et al.*, 2008). The thin sand body that underlies the ravinement surface, with its particular meiofauna assemblage and CU trend (Fig. 6D), may be interpreted as a washover fan deposit (Campo *et al.*, 2017).

CPTU characteristics. This facies association is characterized by Qc values of 4 to 10 MPa, mean Fs of about 0.05 MPa, U generally $<u_0$ and FR ranging between 0.5 to 1.5% (Fig. 8A). The lower boundary is sharply marked by an increase in Qc and U (Fig. 8A). Qc and Fs rapidly decrease upward, whereas U and FR increase in the same direction (Fig. 8A). Locally, the opposite tendency is recorded (Fig. 8A, about 22 m depth).

Qc and FR values reflect a sandy texture (Styllas, 2014). Sedimentary units with high Qc and Fs, low U, and decreasing upward FR and Qc values (FU trend) typify transgressive barrier island deposits, whereas units with lower Qc and Fs, higher U, and increasing upward FR and Qc may represent washover fan deposits with CU grain-size tendency.

Beach ridge/Delta front facies association
Facies characteristics. This facies association is composed of grey to brownish fine to coarse sand, with gradational base, general CU trend and thickness ranging between 2.5 m and 10 m (Figs 2, 6C and 6D). It forms a laterally extensive (up to 100 km) sediment body parallel to the modern shoreline (Campo *et al.*, 2020b). Due to poor preservation of sedimentary structures in cores, two main lithofacies can be identified, mostly on the basis of the fossil content and of accessory materials. Lithofacies 1 is made of highly fossiliferous sand (Fig. 6C); whereas lithofacies 2 includes only rare bioclasts and scattered plant debris (Fig. 6D). In lithofacies 1, molluscs exhibit a varied fauna including *Tritia neritea* and *Chamelea gallina*. On the other hand, the meiofauna is generally poorly-preserved and only few specimens of foraminifera (*Ammonia beccarii* and *Pontocythere turbida*) have been identified (Amorosi *et al.*, 2017b). Lithofacies 2 is characterized by a highly specialized mollusc fauna, with *Lentidium*
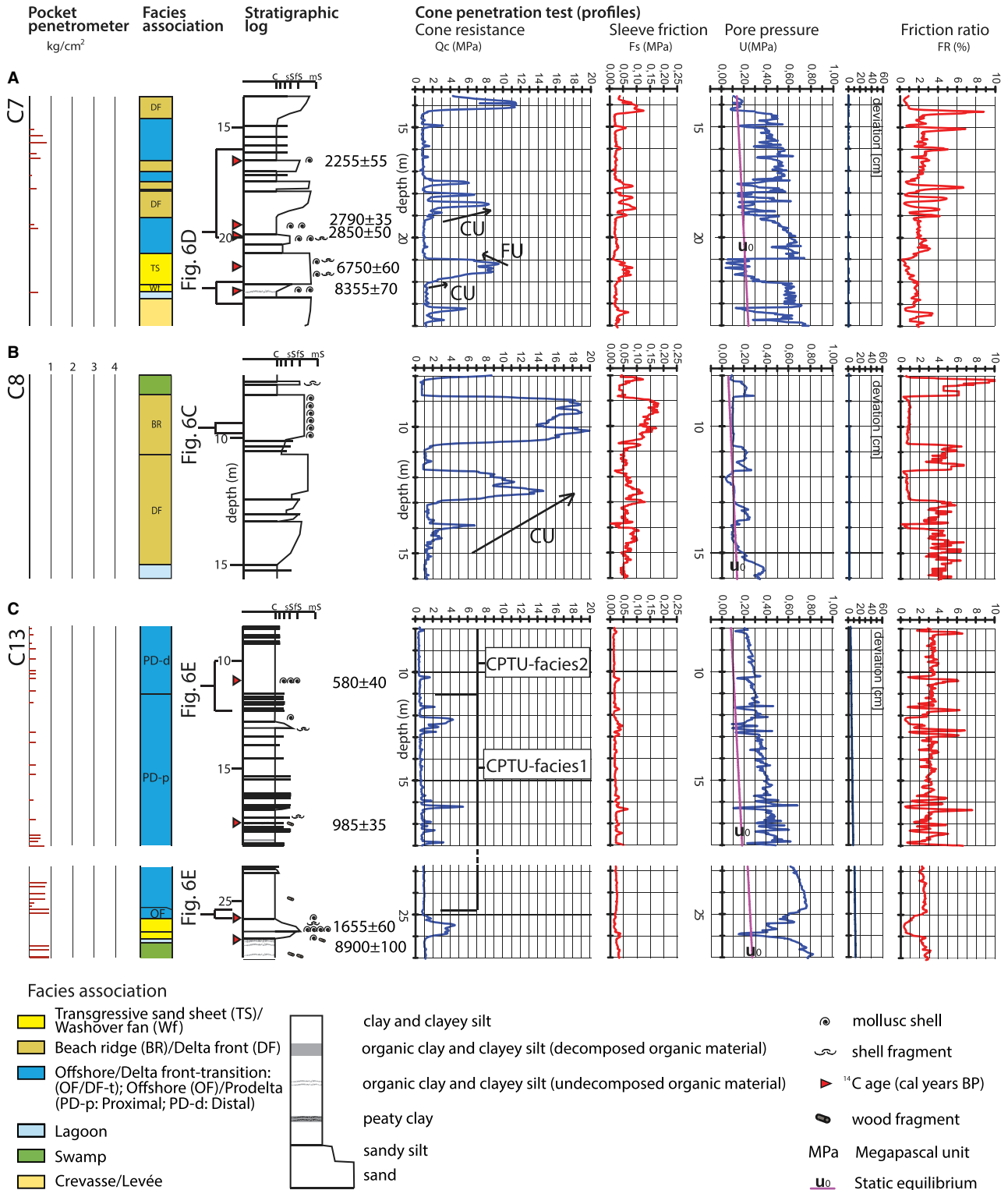
Fig. 8. Identification of nearshore and shallow-marine facies associations in CPTU profiles (Qc, Fs, U and FR) and adjacent cores C7 (A), C8 (B) and C13 (C) (see Fig. 1 for location). FU, fining-upward trend; CU, coarsening-upward trend.

mediterraneum as the main specimen (Scarponi & Angeletti, 2008). The meiofauna is almost absent and represented by opportunistic foraminifera (*Ammonia tepida* and *Palmoconcha turbida*).

The lithology, general CU trend and geometry of this facies association are consistent with sheet sands formed in a high-energy coastal palaeoenvironment during Po Delta progradation. Fossiliferous sands (lithofacies 1), including a mixture of nearshore taxa, are inferred to have been deposited along beach ridges by wave action and longshore currents (Bhattacharya & Giosan, 2003). In lithofacies 2, the abundance of *Lentidium mediterraneum* and of an opportunistic fauna tolerant to high amounts of riverine organic matter is more consistent with highly-stressed environmental conditions, typical of a delta-front environment, where sedimentation is mostly influenced by river activity (Bhattacharya & MacEachern, 2009; Bohacs *et al.*, 2014). Thick and amalgamated sand bodies are inferred to have been deposited close to the shoreline, where the energy of waves and river currents is stronger; basinward, where the transport energy weakens, sand bodies thin out and can be sandwiched within shallow-marine muds (Fig. 2).

CPTU characteristics. This facies association is typified by Q_c values ranging between 4 and 11 MPa (locally up to 20 MPa; Fig. 8A, 8B and Table 1). Fs is generally <0.1 MPa, $U < u_0$ and FR < 1% (Fig. 8A). Q_c values may show an overall upward increase (Fig. 8A and B). The lower boundary is frequently marked by a consistent increase of Q_c (+2/+10 MPa, Fig. 8A), whereas the top is generally sharp (Fig. 8A and B).

Q_c and FR values are typical of both delta-front and beach-ridge facies (Lafuerza *et al.*, 2005) and show no obvious distinction between river-influenced and wave-dominated systems. Increasing upward values of Q_c reflect the overall CU grain-size trend, which is characteristic of coastal (deltaic and strandplain) progradation under highstand conditions.

Shallow-marine deposits

This group includes shallow-marine facies associations observed in the distal sector of the Holocene Po coastal Plain succession (Fig. 2).

Offshore/Delta front transition facies association
Facies characteristics. This facies association is composed of grey silty clay with millimetre to centimetre-thick sand intercalations (Fig. 6D). Its thickness ranges between 1 m and 3 m. Bioturbation is common. Based on the fossil content and stratigraphic position, this facies association can be subdivided into two lithofacies. In lithofacies 1, which generally overlies transgressive sands (Figs 2 and 8A), the meiofauna is characterized by infralittoral and epiphytic species associated with molluscs, such as *Chamelea gallina* and *Antalis inaequicostata*. In the overlying lithofacies 2, which shows upward transition to delta-front deposits (Fig. 2), *Lembulus pella* and *varicorbula gibba* are the main components of the mollusc assemblage (Scarponi & Angeletti, 2008), whereas the meiofauna consists of rare *Ammonia* (*tepida* and *parkinsoniana*) and *Polmoconcha turbida*. Plant debris are locally encountered.

The characteristic alternation of sand–mud layers, the diagnostic fossil content, and stratigraphic position between transgressive barrier sands (below) and prograding nearshore sand bodies (above), suggest the transition between coastal and shallow-marine depositional environments. Palaeontological data allow the further distinction between shoreface–offshore transition deposits (lithofacies 1) and delta-front transition deposits (lithofacies 2). Opportunistic species, in particular, characterize delta-front transition setting because of highly stressed conditions due to riverine influence (Dasgupta *et al.*, 2020).

CPTU characteristics. This facies association is characterized by scarcely rectilinear to seesaw-like CPTU profiles (Fig. 8A). Q_c ranges between 0.9 to 1.5 MPa, with peaks up to 8 MPa (Table 1). Fs and FR range between 0.02 to 0.1 MPa, and 1 to 7%, respectively. U has typically positive values, though locally negative (or $<u_0$) values can be encountered (Table 1).

Q_c and FR values are indicative of a heterolithic facies association with dominant muds and subordinate fine sand (Robertson, 2010), in accordance with the interpretation of this facies association as an offshore-delta front transition. The distinction between offshore-transition and delta-front transition lithofacies is not possible based on CPTU data alone.

Offshore/Prodelta facies association
Facies characteristics. This facies association, up to 20 m thick (Fig. 2), is composed of three vertically-stacked lithofacies (Fig. 5E): lithofacies 1 consists of homogeneous and bioturbated grey clay, about 0.5 m thick (Fig. 6E). Lithofacies 2 is made of organic-matter-rich silty clay, with

millimetre to decimetre-thick silty sand intercalations (Fig. 6E). Sand intervals are thicker and more frequent upward. Lithofacies 3 is characterized by darkish grey organic-rich clay coarsening upward to silt (Fig. 6E). Distinct fossil assemblages typify these lithofacies (Amorosi *et al.*, 2017b): the faunal content in lithofacies 1 displays *Timoclea ovata* and *Bittium submammillatum* mollusc shells, along with open-marine and epiphytic taxa. Lithofacies 2 is mostly barren of macrofossils and dominated by *Ammonia* (*tepida* and *parkinsoniana*) and *Palmoconcha turbida*. In lithofacies 3 *Corbula gibba* and *Turritella communis* are diagnostic molluscs (Fig. 6D). The meiofauna is characterized by *Nonionella turgida*, *Valvulineria bradyana* and *Bulimina marginata*.

Lithology, sedimentological features and palaeontological data denote a shallow-marine environment (Dasgupta *et al.*, 2020). In lithofacies 1, the dominance of clay, combined with a diversified meiofauna and the relative abundance of open-marine species are consistent with an offshore setting. The dominance of silt (lithofacies 2) or clay (lithofacies 3), in association with a mostly opportunistic meiofauna, is indicative of proximal versus distal prodelta environments, respectively. This further distinction is also supported by the relative abundance of *Nonionella turgida*, which is an indicator of distal prodelta settings (Barbieri *et al.*, 2021).

CPTU characteristics. This facies association is characterized by low values of Qc and Fs, ranging between 0.3 to 1.0 MPa and 0.01 to 0.025 MPa, respectively (Fig. 8C). In particular, two distinct CPTU-facies can be recognized: CPTU-facies 1, with Qc of 0.6 to 1.0 MPa and Fs of about 0.025 MPa; and CPTU-facies 2, with slightly lower Qc and Fs values (Qc: 0.3–0.6 MPa and Fs: 0.01–0.025 MPa; Fig. 8C). Subordinate peaks in both of the curves are in the order of 1.2 to 5.0 MPa (Qc) and 0.03 to 0.05 MPa (Fs; Fig. 8C). Peaks in Qc are relatively more frequent in CPTU-facies 1, where profiles show a typical seesaw shape. A similar trend is recorded by the FR profile, with values ranging between 2.0 to 3.5% for CPTU-facies 1 and between 3% and 4% upward for CPTU-facies 2 (Fig. 8C). U commonly has positive values ($>u_0$), ranging between 0.2 to 0.3 MPa for CPTU-facies 2, and between 0.3 to 0.75 MPa for CPTU-facies 1 (Fig. 8C). The latter locally shows $<u_0$ (Fig. 8C and Table 1).

Based on geotechnical characteristics, this facies association can be divided into two distinct CPTU-facies: the basal CPTU-facies 1 (25–11.5 m

depth, Fig. 8C), with relatively higher Qc, Fs and U, and lower FR than the overlying (11.5–8.0 m depth, Fig. 8C) CPTU-facies 2.

Similar Qc and FR have been reported from fine-grained prodelta sediments (Lafuerza *et al.*, 2005; Zhang *et al.*, 2018). Characteristic Qc, Fs and FR values between CPTU-facies 1 and 2 are consistent with proximal and distal prodelta lithofacies, respectively, identified in cores. On the other hand, the distinction between offshore and distal-prodelta deposits cannot be accomplished on the basis of CPTU measurements alone.

DISCUSSION

Facies associations and the soil behaviour type chart

The 12 facies associations characterized in terms of all basic CPT parameters (plus U) were plotted onto the SBT chart of Robertson (2010; Fig. 9) to test if this chart, based on two variables only, can be useful for facies identification well beyond the simple differentiation between sand and mud.

The SBT chart includes nine different soil behaviour zones, each defined by particular Qc and FR thresholds (Fig. 9). Each zone groups soil types using traditional lithological descriptions (i.e. clay and sand). This updated chart can be helpful for real-time data processing and interpretation during CPT and/or CPTU procedures, especially in predominantly silica-based, young (i.e. Upper Pleistocene–Holocene) and uncemented soil (i.e. ideal soil).

The Po Plain facies associations were plotted onto three different SBT charts, corresponding to continental (alluvial plain – Fig. 9A), transitional (estuary and delta plain – Fig. 9B) and marine (nearshore/delta front and shallow-marine/prodelta) depositional systems (Fig. 9C). Fluvial/distributary-channel (Fig. 9A) and bay-head delta (Fig. 9B) facies display the highest Qc values, and plot mostly in zone 6 ('sand deposits', Robertson, 2010), only locally trespassing into zone 7 (dense sand to gravelly sand). Beach-ridge/delta-front facies plot in zone 6 (Fig. 9C) and partially in zone 5 (silty sand to sandy silt). This latter includes crevasse (Fig. 9A) and transgressive barrier/washover fan deposits (Fig. 9C). Levée deposits are lithologically finer-grained and plot mostly into zone 4 ('silt mixtures', Fig. 9A). The lagoonal facies covers a relatively wide spectrum of lithologies (Fig. 9B), from outer lagoon 'sand mixtures'
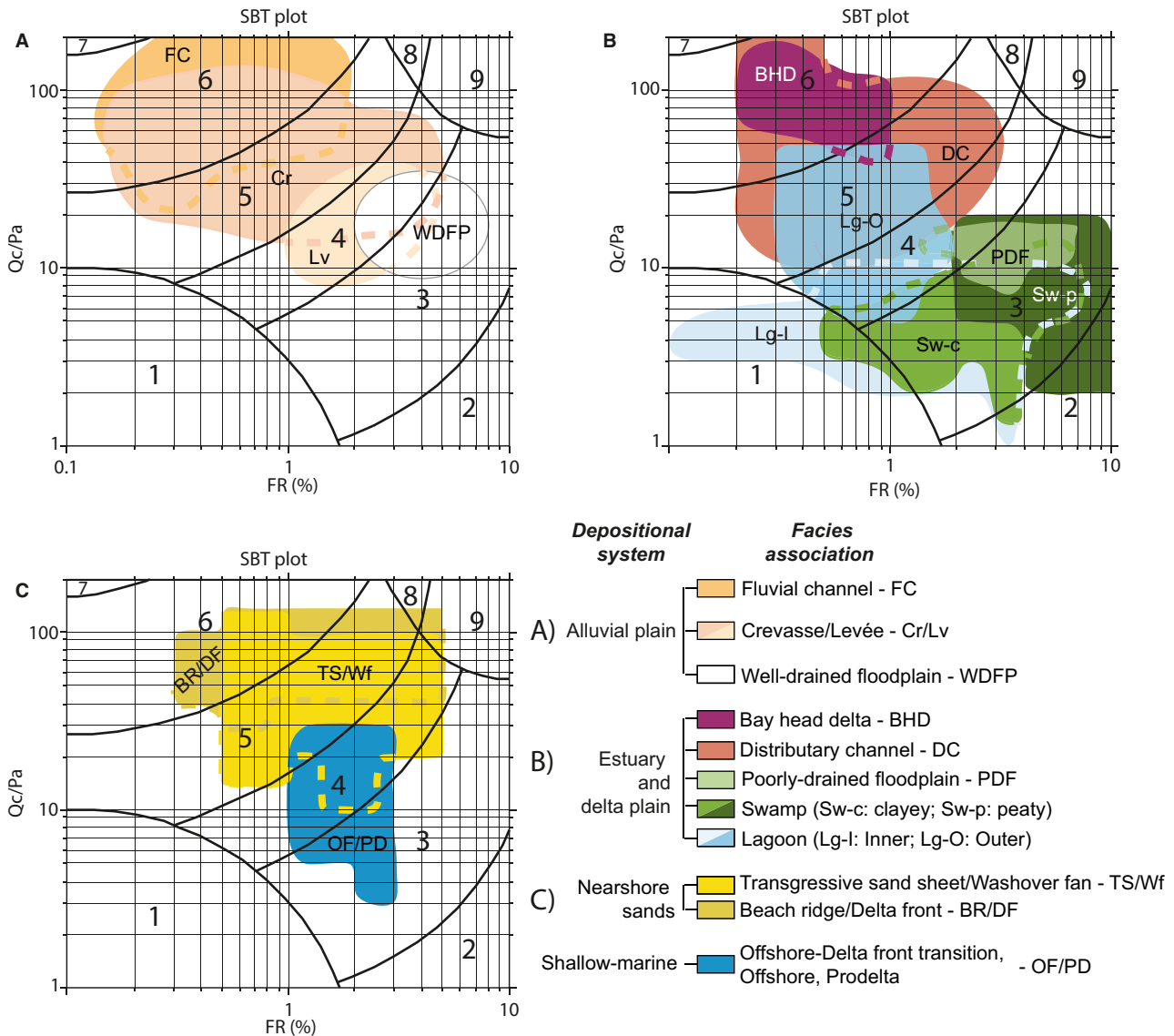
Fig. 9. Plots of facies associations onto the soil behaviour type (SBT) chart of Robertson (2010). (A) Alluvial plain facies associations. (B) Estuarine and lower delta plain facies associations. (C) Nearshore and shallow-marine facies associations. Zone 1: Sensitive fine-grained; Zone 2: Clay-organic soil; Zone 3: Clays: clay to silty clay; Zone 4: Silt mixtures: clayey silt and silty clay; Zone 5: Sand mixtures: silty sand to sandy silt; Zone 6: Sands: clean sands to silty sands; Zone 7: Dense sand to gravelly sand; Zone 8: Stiff sand to clayey sand (overconsolidated or cemented); Zone 9: Stiff fine-grained (overconsolidated or cemented). Dimensionless cone resistance: Qc/Pa, where Pa = 1 bar (or 0.1 MPa). FR, Friction ratio.

(zone 5) to inner lagoon 'sensitive fine-grained' sediments (zone 1). The offshore/prodelta facies association is mainly classified as 'silt mixtures' (zones 4–3; Fig. 9C). Fine-grained facies associations generally plot between zones 3 ('clay to silty clay') and 1, only occasionally in zone 4 (Fig. 9). Well-drained and poorly-drained floodplain deposits belong to the silty clay facies (zones 4–3), whereas swamp deposits fall mostly within

zone 3. Swamp clay is locally represented by 'sensitive fine-grained' zone 1 deposits, whereas swamp peat partially falls in zone 2 ('organic-soil' – Fig. 9B).

Plotting sedimentary facies into SBT charts results in the clear lithological distinction between coarse-grained and fine-grained deposits. Coarse-grained facies show typically high (>4 MPa) Qc and low (<2%) FR, and generally

plot in zone 6, whereas fine-grained deposits fall into zones 3–1, because of low Qc (<2.5 MPa) and high (>3%) FR. Heterolithic facies associations plot within intermediate zones 4 and 5.

The SBT chart may provide accurate prediction of sediment type, but this is not straightforward, and more parameters need to be considered to accurately characterize facies associations from different depositional systems (Styllas, 2014). Besides lithology, the concept of sedimentary facies involves additional features, which are strictly related to their geological history. Since facies associations are genetically linked to their depositional system, each deposit depends on depositional conditions, but also on post-depositional processes (Truong *et al.*, 2011; Maliva, 2016). This 'genetic link' makes the use of sequence stratigraphic concepts as an ideal complementary tool for CPTU interpretation. In this regard, the comparison of SBT charts locally shows significant overlap (see dashed lines in Fig. 9) of CPTU characteristics among facies associations from different depositional systems. This is due to the fact that different facies have similar engineering properties and are made of the same lithology. However, sedimentary facies can be characterized by distinctive grain-size trends (FU, CU), U ranges (<0, >0), thickness, gradational/sharp/erosional contacts and diagnostic peaks in CPTU curves. For this reason, the SBT charts cannot be utilized for accurate facies identification if sedimentary facies have the same lithology (and similar mechanical behaviour). For example, fluvial-channel and bay-head delta sands both plot on class 6 (Fig. 9A and B). In this case, FU or CU trends may be helpful for their distinction. These trends are very well-expressed by CPT/CPTU curves (Figs 3, 5, 7 and 8), but unavailable in the SBT charts (Fig. 9). Similarly, for swamp deposits, concomitant peaks in Qc, Fs, U and FR curves are diagnostic of peat deposits (Fig. 7B). Thus, interpretation of CPT/CPTU curves using sedimentological concepts is a much more effective tool for high-resolution facies identification than SBT charts alone. Where distinct sedimentary facies exhibit remarkable overlap onto the SBT chart, such as for swamp, lagoon and prodelta deposits (Fig. 9B and C), CPTU test interpretation is largely insufficient to refine facies characterization. Even though U values may be slightly different (but generally positive) for these three facies associations, lagoon and prodelta deposits locally showing <u_0 (Table 1), variations of pore pressure alone do not allow for their recognition. In such instances, calibration of CPTU data with detailed facies analysis from sediment cores and sequence stratigraphic concepts can be used to predict proximal to distal facies relationships. As facies accumulation is mostly a function of the interaction between accommodation space and sediment supply (Posamentier *et al.*, 1988; Van Wagoner *et al.*, 1990; Muto & Steel, 1997) and facies distribution is strongly related to systems tract architecture (for example, estuarine deposits are typically developed in TST; prodelta and delta front in HST/LST; amalgamated fluvial bodies in LST; Shanley & McCabe, 1991; Allen & Posamentier, 1994; Cattaneo & Steel, 2003; see Fig. 2) the sequence stratigraphic approach can enhance interpretation of CPTU data, allowing reliable interpretation of deposits that may show nearly identical lithological characteristics.

The CPTU data may also reveal specific characteristics undetected in cores because of recovery issues. Grain-size trends and centimetre to decimetre mud intercalations within sand deposits can easily get lost during core recovery with the rotary wash drilling method. Furthermore, sand recovery is not easy to accomplish during routine drilling operations, unless special and expensive equipment is utilized. For example, silty clay intercalations can be present within beach-ridge deposits (or within other sand bodies, such as the bay-head delta in Figs 2 and 7B). This stratigraphic information could be lost during core recovery. Amorosi *et al.* (2017b) utilized CPTU profiles to identify flooding surfaces within Holocene strata (Fig. 2), proving that similar information can be precious for high-resolution stratigraphic analysis. In this regard, Monahan (1999) noticed that sharp versus gradational lithological boundaries, CU/FU sequences and dips in foreset beds could be recognized beyond the limits of borehole control. Similarly, Törnqvist *et al.* (2000) showed the potential of CPT data to identify marked facies transitions not recovered in the core.

As a whole, CPTU interpretation is as an effective tool for the characterization of fine-grained alluvial, paralic and shallow-marine facies associations for which sedimentological characterization can be difficult. Since CPT and CPTU are fast and economical tests, they can be used for preliminary investigations of late Pleistocene–Holocene strata in order to evaluate and plan additional (more expensive) geological tests.

This CPT/CPTU approach can reasonably be exported to similar settings worldwide as several delta and coastal plain successions share

comparable post-LGM stratigraphic architectures and stratal thickness (Hori *et al.*, 2002; Tanabe *et al.*, 2006; Hijma *et al.*, 2009; Styllas, 2014; He *et al.*, 2020) in response to eustatic sea-level rise, with only minor differences between microtidal and macrotidal areas (Zhang *et al.*, 2018).

Application of CPTU-facies identification to subsurface investigation of alluvial and coastal plains

The concept of sedimentary facies has become increasingly common among geotechnical engineers. Because of the spatial variability of subsurface geomechanical behaviour and its potential influence on differential ground settlements, a sedimentary facies approach can be highly useful for mapping, modelling and predict consolidation of late Quaternary deposits, especially beneath highly-populated coastal areas, from Europe to Asia (Ricceri *et al.*, 2002; Choi & Kim, 2006; Dipova, 2011). The soil behaviour can be highly influenced by depositional and post-depositional processes (Truong *et al.*, 2011; Sarti *et al.*, 2012). As different facies have distinct geotechnical and geomechanical characteristics (Truong *et al.*, 2013; Lorenzo *et al.*, 2014), facies characterization through CPTU could be utilized

to make predictions about the 3D spatial distribution of geomechanically 'weak' versus 'strong' deposits, aside from any specific geographic location. Through the analysis of CPTU profiles, for example, soft, unconsolidated Holocene deposits with low Qc and Fs can be easily distinguished from stiff (high Qc and Fs) and more consolidated Pleistocene sediments, as shown in Fig. 10. Since Holocene, soft (and organic-rich) deposits typically overlie hardened pedogenized horizons also in several delta plains of Asia, America and Europe (Blum & Aslan, 2006; Choi & Kim, 2006; Bos *et al.*, 2012; Hijma *et al.*, 2017; Fan *et al.*, 2019), this approach can have important applications from an engineering perspective also outside the Po Plain at the global scale.

In geotechnical surveys, the convenience of a facies approach is also suggested by studies on soil liquefaction (Watts *et al.*, 1992; Amorosi *et al.*, 2016) and sediment compaction assessment (Koster *et al.*, 2016). The latter mostly concerns soft (for example, paludal, lagoonal and prodelta) clays, and may be one of the major factors controlling subsidence, as documented by recent research on organic-matter-rich Holocene strata of The Netherlands and Italy (van Asselen *et al.*, 2009; Teatini *et al.*, 2011; Bruno *et al.*, 2020). Considerable volumes of these paludal, estuarine and
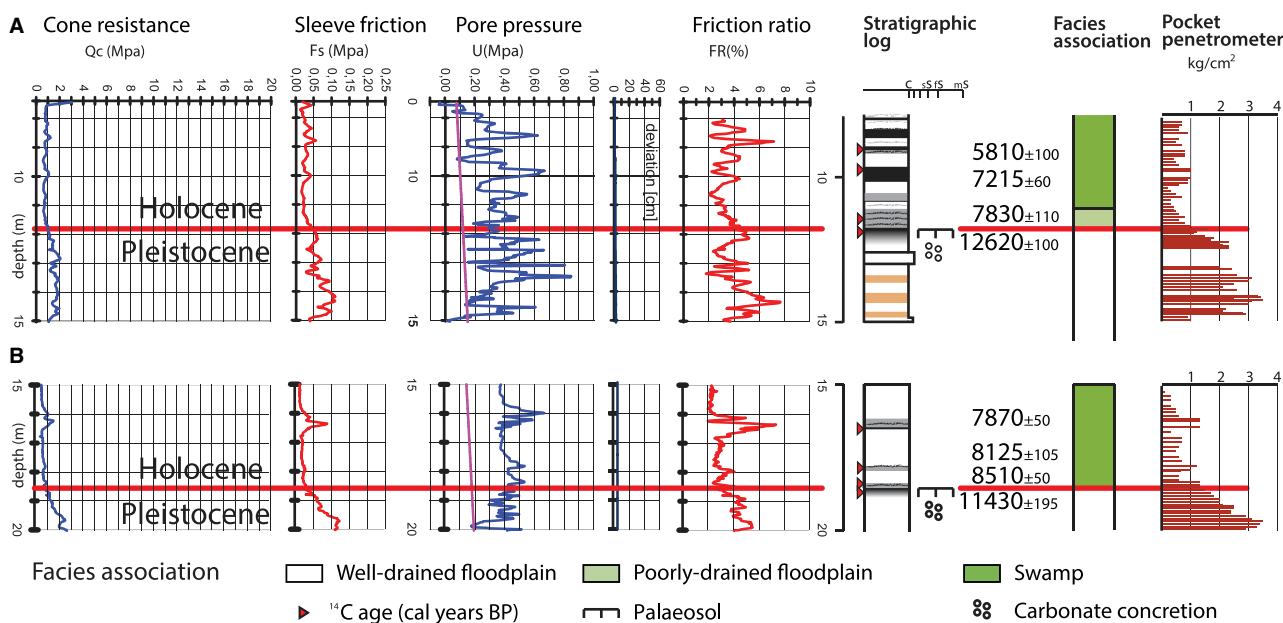
Fig. 10. Recognition of the Pleistocene–Holocene boundary based on CPTU data: (A) core C3; and (B) core C1 (Fig. 1 for location). Stiff, well-drained floodplain Pleistocene facies are overlain by soft poorly-drained to swamp Holocene facies associations. CPTU data are supported by pocket penetration information suggesting a similar geotechnical behaviour. Qc, Cone tip resistance; Fs, Sleeve friction; U, pore water pressure; u₀, static equilibrium pore pressure; FR, Friction Ratio; MPa, Megapascal unit.

prodelta–offshore facies associations are present within Holocene Po Plain strata (Campo *et al.*, 2020a). Similar soft deposits are very common also beneath other modern delta/coastal plains worldwide, from Europe, Asia and America (Törnqvist *et al.*, 2008; Tanabe *et al.*, 2013, 2015; Zhang *et al.*, 2014, 2021; Sarti *et al.*, 2015; Koster *et al.*, 2018; Zoccarato *et al.*, 2018, 2020; He *et al.*, 2020; Liu *et al.*, 2020). Thus, their recognition and mapping based on simple CPTU investigations might be economically practical and convenient.

Even though basic CPT parameters plus U turned out to be an excellent tool for *in situ* facies characterization, additional data from cone penetration testing could be considered for this purpose. For example, dissipation tests could be used to estimate soil permeability and to assess the correct equilibrium piezometric pressure. As seismic CPTU (SCPTU) tests are also becoming increasingly common, evaluating the potential of additional parameters, such as *in situ* shear wave velocity or compression wave velocity, might be very useful for future CPTU-based facies characterization.

CONCLUSIONS

Engineering geological investigation of unconsolidated late Quaternary deposits through piezocone penetration tests (CPTU) is commonly limited to graphical representation of soil lithology into soil behaviour type (SBT) charts. In the southern Po Plain, where an abundance of sedimentological, palaeontological and chronological data is available, the calibration of CPTU profiles with 20 adjacent continuously cored boreholes demonstrates the strong potential of CPTU analysis for recognition and geotechnical characterization of alluvial, deltaic and coastal facies associations that are common to comparable settings all around the world. In order to visualize the engineering properties of the study units and to test the high potential of the proposed CPTU-based methodology for facies analysis, facies associations were plotted onto the SBT charts using non-normalized (i.e. basic) cone resistance (Qc) and friction ratio (FR).

Major results can be summarized as follows:

• Sand-rich (fluvial/distributary-channel, bay-head delta, transgressive barrier, delta-front/beach-ridge) and mud-dominated (well-drained/poorly-drained floodplain, swamp, lagoonal and prodelta) facies associations have contrasting cone resistance (Qc) and water pore pressure (U) signatures that clearly reflect strong differences in grain size. On the other hand, plotting similar lithologies onto the SBT chart of Robertson (2010) resulted in local overlap between facies associations.

• Despite only subtle differences in grain size, clay-rich and silt-rich facies associations have markedly distinct engineering properties. Within well-drained floodplain deposits, palaeosols exhibit sharp peaks in Qc and Fs, and a general abrupt decrease in U that can be easily detected on CPTU profiles. The swamp facies association can be subdivided into two main CPTU-lithofacies: swamp clays, with characteristic rectilinear CPTU profiles; and swamp peats, typified by concomitant peaks in Qc, Fs, U and FR. Although swamp and lagoon facies associations have similar engineering characteristics, swamp clays and central lagoon facies plot towards the 'sensitive fine-grained' zone 1, whereas swamp peat locally falls into the 'organic-soil' zone 2 and outer lagoon deposits into the 'sand mixtures' zone 5.

• Although the SBT chart offers good prediction of sediment type, parameters other than basic Qc and FR values can improve facies characterization, including Qc and Fs trends, negative/positive pore pressures, thickness values, gradational versus sharp bases/tops and characteristic peaks in CPTU profiles.

• In some instances, distinct facies associations may overlap onto the soil behaviour type chart and cannot be identified through CPTU analysis. In such instances, accurate facies analysis on sediment cores and sequence stratigraphic concepts are required to predict proximal to distal facies relationships and guide stratigraphic correlation.

• CPTU data may also reveal specific characteristics undetected in cores because of recovering issues, such as grain-size tendencies and centimetre to decimetre thick mud intercalations within sand deposits that may represent important stratigraphic surfaces.

• This study offers a methodology for CPTU profiles interpretation that can be confidently used for identification of facies association and for a variety of applications (stratigraphic correlation, hydrogeological, geotechnical and engineering investigations) in alluvial, coastal and deltaic settings worldwide because of similar late Quaternary stratigraphic architecture. After calibration with a limited number of cores,

CPTU can be useful to increase data coverage at reasonable costs. This methodology can be complementary to the soil texture classification of the SBT charts and is particularly recommended for *in situ* facies association recognition, no matter where alluvial and/or coastal unconsolidated successions are located in the world.

ACKNOWLEDGEMENTS

DATA AVAILABILITY STATEMENT

The CPTU profiles used in this work are part of the subsurface database of the Emilia-Romagna Geological, Seismic and Soil Survey, freely accessible online at https://applicazioni.regione.emilia-romagna.it/cartografia_sgss/user/viewer.jsp?service=geologia. Additional data (continuous cores: C cores) that support the findings of this study are available from the corresponding author upon reasonable request.

REFERENCES

Allen, G.P. and **Posamentier, H.W.** (1994) Transgressive facies and sequence architecture in mixed tide-and wave-dominated incised valleys: example from the Gironde estuary, France. In: *Incised-Valley Systems: Origin and Sedimentary Sequences* (Eds Dalrymple, R.W., Boyd, B.R. and Zaitlin, B.A.), *SEPM Special Publication*, **51**, 225–240.

Amorosi, A. and **Marchi, N.** (1999) High-resolution sequence stratigraphy from piezocone tests: an example from the late quaternary deposits of the southeastern Po plain. *Sediment. Geol.*, **128**, 67–81.

Amorosi, A., **Colalongo, M.L.**, **Fiorini, F.**, **Fusco, F.**, **Pasini, G.**, **Vaiani, S.C.** and **Sarti, G.** (2004) Palaeogeographic and palaeoclimatic evolution of the Po plain from 150-ky core records. *Glob. Planet. Change*, **40**, 55–78.

Amorosi, A., **Bruno, L.**, **Campo, B.** and **Morelli, A.** (2015) The value of pocket penetration tests for the high-resolution palaeosol stratigraphy of late quaternary deposits. *Geol. J.*, **50**, 670–682.

Amorosi, A., **Bruno, L.**, **Facciorusso, J.**, **Piccin, A.** and **Sammartino, I.** (2016) Stratigraphic control on earthquake-induced liquefaction: a case study from the Central Po plain (Italy). *Sediment. Geol.*, **345**, 42–53.

Amorosi, A., **Bruno, L.**, **Cleveland, D.M.**, **Morelli, A.** and **Hong, W.** (2017a) Paleosols and associated channel-belt sand bodies from a continuously subsiding late quaternary system (Po basin, Italy): new insights into continental sequence stratigraphy. *Bull. Geol. Soc. Am.*, **129**, 449–463.

Amorosi, A., **Bruno, L.**, **Campo, B.**, **Morelli, A.**, **Rossi, V.**, **Scarponi, D.**, **Hong, W.**, **Bohacs, K.M.** and **Drexler, T.M.** (2017b) Global Sea-level control on local parasequence architecture from the Holocene record of the Po plain, Italy. *Mar. Pet. Geol.*, **87**, 99–111.

Amorosi, A., **Barbieri, G.**, **Bruno, L.**, **Campo, B.**, **Drexler, T.M.**, **Hong, W.**, **Rossi, V.**, **Sammartino, I.**, **Scarponi, D.** and **Vaiani, S.C.** (2019) Three-fold nature of coastal progradation during the Holocene eustatic highstand, Po plain, Italy–close correspondence of stratal character with distribution patterns. *Sedimentology*, **66**, 3029–3052.

Amorosi, A., **Bruno, L.**, **Campo, B.**, **Costagli, B.**, **Dinelli, E.**, **Hong, W.**, **Sammartino, I.** and **Vaiani, S.C.** (2020) Tracing clinothem geometry and sediment pathways in the prograding Holocene Po Delta system through integrated core stratigraphy. *Basin Res.*, **32**, 206–215.

Amorosi, A., **Bruno, L.**, **Campo, B.**, **Costagli, B.**, **Hong, W.**, **Picotti, V.** and **Vaiani, S.C.** (2021) Deformation patterns of upper quaternary strata and their relation to active tectonics, Po Basin, Italy. *Sedimentology*, **68**, 402–424.

van Asselen, S., **Stouthamer, E.** and **van Asch, T.W.J.** (2009) Effects of peat compaction on delta evolution: a review on processes, responses, measuring and modeling. *Earth-Science Rev.*, **92**, 35–51.

Barbieri, G., **Rossi, V.**, **Vaiani, S.C.**, **Dasgupta, U.** and **Amorosi, A.** (2021) Quantitative paleoecology in shallow-marine settings: the value of ostracods and foraminifers from the Holocene north Adriatic record. *Palaeogeogr. Palaeoclimatol. Palaeoecol.*, **572**, 110408.

Bates, M.R., **Bates, C.R.** and **Whittaker, J.E.** (2007) Mixed method approaches to the investigation and mapping of buried quaternary deposits: examples from southern England. *Archaeol. Prospect.*, **14**, 104–129.

Beets, D.J., **Roep, T.B.** and **Westenrhoff, W.E.** (1996) The holocene bergen inlet: closing history and related barrier progradation. In: *Coastal Studies on the Holocene of the Netherlands*, pp. 97–131. Boom-Planeta, Haarlem.

Begemann, H.K. (1965) The friction jacket cone as an aid in determining the soil profile. *Proc. 6th Int. Conf. on SMFE*, **1**, 17–20.

Berry, K.M., **Olson, S.M.** and **Lamie, M.** (1998) Cone penetration testing in the Mid-Mississippi River Valley. In: *Geotechnical Site Characterization* (Eds Robertson, P.K. and Mayne, P.W.), pp. 983–987. Balkema, Rotterdam.

Bhattacharya, J.P. (2006) Deltas. In: *Facies Models Revisited* (Eds Walker, R.G. and Posamentier, H.), *SEPM Spec. Publ*, **84**, 237–292.

Bhattacharya, J.P. and **Giosan, L.** (2003) Wave-influenced deltas: geomorphological implications for facies reconstruction. *Sedimentology*, **50**, 187–210.

Bhattacharya, J.P. and **MacEachern, J.A.** (2009) Hyperpycnal rivers and prodeltaic shelves in the cretaceous seaway of North America. *J. Sediment. Res.*, **79**, 184–209.

Blum, M.D. and **Aslan, A.** (2006) Signatures of climate vs. sea-level change within incised valley-fill successions: quaternary examples from the Texas GULF coast. *Sediment. Geol.*, **190**, 177–211.

Boccaletti, M., **Corti, G.** and **Martelli, L.** (2011) Recent and active tectonics of the external zone of the northern Apennines (Italy). *Int. J. Earth Sci.*, **100**, 1331–1348.

Bohacs, K.M., **Lazar, O.R.** and **Demko, T.M.** (2014) Parasequence types in shelfal mudstone strata—quantitative observations of lithofacies and stacking patterns, and conceptual link to modern depositional regimes. *Geology*, **42**, 131–134.

Bos, I.J., **Busschers, F.S.** and **Hoek, W.Z.** (2012) Organic-facies determination: a key for understanding facies distribution in the basal peat layer of the Holocene Rhine-Meuse delta, The Netherlands. *Sedimentology*, **59**, 676–703.

Boyd, R., **Dalrymple, R.W.** and **Zaitlin, B.A.** (2006) Estuarine and incised-valley facies models. In: *Facies Models Revisited* (Eds Posamentier, H.W. and Walker, R.G.), *SEPM Spec. Publ*, **84**, 171–235.

Bridge, J.S. (1984) Large-scale facies sequences in alluvial overbank environments. *J. Sediment. Petrol.*, **54**, 583–588.

Bruno, L., **Bohacs, K.M.**, **Campo, B.**, **Drexler, T.M.**, **Rossi, V.**, **Sammartino, I.**, **Scarponi, D.**, **Hong, W.** and **Amorosi, A.** (2017) Early Holocene transgressive palaeogeography in the Po coastal plain (northern Italy). *Sedimentology*, **64**, 1792–1816.

Bruno, L., **Amorosi, A.** and **Di Martino, A.** (2019) Peat layer accumulation and post - burial deformation during the mid - late Holocene in the Po coastal plain (northern Italy). *Basin Res.*, **31**, 621–639.

Bruno, L., **Campo, B.**, **Costagli, B.**, **Stouthamer, E.**, **Teatini, P.**, **Zoccarato, C.** and **Amorosi, A.** (2020) Factors controlling natural subsidence in the Po plain. *Proc. Int. Assoc. Hydrol. Sci.*, **382**, 285–290.

Bruno, L., **Campo, B.**, **Hajdas, I.**, **Hong, W.** and **Amorosi, A.** (2022) Timing and mechanisms of sediment accumulation and pedogenesis: insights from the Po plain (northern Italy). *Palaeogeogr. Palaeoclimatol. Palaeoecol.*, **591**, 110881.

Buol, S.W., **Southard, R.J.**, **Graham, R.C.** and **McDaniel, P.A.** (2011) *Soil Genesis and Classification*, 6th edn. John Wiley & Sons, Ames, 560 pp.

Burrato, P., **Ciucci, F.** and **Valensise, G.** (2003) An inventory of river anomalies in the Po plain, northern Italy: evidence for active blind thrust faulting. *Ann. Geophys.*, **46**, 865–882.

Cacciari, M., **Rossi, V.**, **Marchesini, M.**, **Amorosi, A.**, **Bruno, L.** and **Campo, B.** (2018) Palynological characterization of the Po delta succession (northern Italy): Holocene vegetation dynamics, stratigraphic patterns and palaeoclimate variability. *Alp. Mediterr. Quat.*, **31**, 109–112.

Campo, B., **Amorosi, A.** and **Vaiani, S.C.** (2017) Sequence stratigraphy and late quaternary paleoenvironmental evolution of the northern Adriatic coastal plain (Italy). *Palaeogeogr. Palaeoclimatol. Palaeoecol.*, **466**, 265–278.

Campo, B., **Amorosi, A.** and **Bohacs, K.M.** (2020a) Late quaternary sequence stratigraphy as a tool for groundwater exploration: lessons from the Po River basin (northern Italy). *Am. Assoc. Pet. Geol. Bull.*, **104**, 681–710.

Campo, B., **Bruno, L.** and **Amorosi, A.** (2020b) Basin-scale stratigraphic correlation of late Pleistocene-Holocene (MIS 5e-MIS 1) strata across the rapidly subsiding Po Basin (northern Italy). *Quat. Sci. Rev.*, **237**, 106300.

Carminati, E. and **Doglioni, C.** (2012) Alps vs. Apennines: the paradigm of a tectonically asymmetric earth. *Earth-Sci. Rev.*, **112**, 67–96.

Cattaneo, A. and **Steel, R.J.** (2003) Transgressive deposits: a review of their variability. *Earth-Sci. Rev.*, **62**, 187–228.

Choi, K. and **Kim, J.H.** (2006) Identifying late quaternary coastal deposits in Kyonggi Bay, Korea, by their geotechnical properties. *Geo-Marine Lett.*, **26**, 77–89.

Coerts, A. (1996) *Analysis of Static Cone Penetration Test Data for Subsurface Modelling: A Methodology*. Koninklijk Nederlands Aardrijkskundig Genootschap, Utrecht.

Curzi, P.V., **Tonni, L.**, **Gottardi, G.** and **Mandanici, E.** (2017) High resolution sedimentological and geotechnical characterization of the late quaternary deposits in the Italian central Adriatic coast (Tronto River mouth). *Eng. Geol.*, **220**, 219–233.

Dafalla, M., **Shaker, A.**, **Elkady, T.**, **Almajed, A.** and **Al-Shamrani, M.** (2020) Shear strength characteristics of a sand clay liner. *Sci. Rep.*, **10**, 1–10.

Dalrymple, R.W., **Zaitlin, B.A.** and **Boyd, R.** (1992) Estuarine facies models; conceptual basis and stratigraphic implications. *J. Sediment. Res.*, **62**, 1130–1146.

Dasgupta, U., **Barbieri, G.**, **Vaiani, S.C.** and **Ghosh, A.** (2020) Potential and limits of benthic foraminiferal ecological indices in paleoenvironmental reconstructions: a case from a Holocene succession of the Po Delta, Italy. *Micropaleontology*, **66**, 103–126.

Devincenzi, M.J., **Colas, S.**, **Casamor, J.L.**, **Canals, M.**, **Falivene, O.** and **Busquets, P.** (2003) Aplicación del piezocono para el estudio sedimentológico de detalle de los sedimentos cuaternarios del Delta del Llobregat, Barcelona. In: *Proceedings III Congreso Andaluz de Carreteras, Sevilla, España*.

Devincenzi, M., **Colas, S.**, **Casamor, J.L.**, **Canals, M.**, **Falivene, O.** and **Busquets, P.** (2004) High resolution stratigraphic and sedimentological analysis of Llobregat delta nearby Barcelona from CPT & CPTU Tests. In: *Proc. 2nd International Conference on Geotechnical Site Characterization ISC-2, Porto*.

Dipova, N. (2011) Geotechnical characterization and facies change detection of the Bogacay coastal plain (Antalya, Turkey) soils. *Environ. Earth Sci.*, **62**, 883–896.

Facciorusso, J., **Madiai, C.** and **Vannucchi, G.** (2015) CPT-based liquefaction case history from the 2012 Emilia earthquake in Italy. *J. Geotech. Geoenvironmental Eng.*, **141**, 5015002.

Fan, D., **Shang, S.** and **Burr, G.** (2019) Sea level implications from late quaternary/holocene paleosols from the Oujiang Delta, China. *Radiocarbon*, **61**, 83–99.

Flach, G.P., **Harris, M.K.**, **Smits, A.D.** and **Syms, F.H.** (2005) Modeling aquifer heterogeneity using cone penetration testing data and stochastic upscaling methods. *Environ. Geosci.*, **12**, 1–15.

Gu, X., **Jiang, Y.** and **Zhou, L.** (2021) The application of piezocone penetration test (CPTU) in water area hydrogeological investigation. In: *E3S Web of Conferences*, Vol. **236**, p. 1039. EDP Sciences.

Gueting, N., **Klotzsche, A.**, **van der Kruk, J.**, **Vanderborght, J.**, **Vereecken, H.** and **Englert, A.** (2015) Imaging and characterization of facies heterogeneity in an alluvial aquifer using GPR full-waveform inversion and cone penetration tests. *J. Hydrol.*, **524**, 680–695.

He, L., **Amorosi, A.**, **Ye, S.**, **Xue, C.**, **Yang, S.** and **Laws, E.A.** (2020) River avulsions and sedimentary evolution of the Luanhe fan-delta system (North China) since the late Pleistocene. *Mar. Geol.*, **425**, 106194.

Helfensdorfer, A.M., **Power, H.E.** and **Hubble, T.C.T.** (2020) Atypical responses of a large catchment river to the Holocene Sea-level highstand: the Murray River, Australia. *Sci. Rep.*, **10**, 1–15.

Hijma, M.P., **Cohen, K.M.**, **Hoffmann, G.**, **Van der Spek, A.J.** and **Stouthamer, E.** (2009) From river valley to estuary: the evolution of the Rhine mouth in the early to middle

Holocene (western Netherlands, Rhine-Meuse delta). *Netherlands J. Geosci.*, **88**, 13–53.

Hijma, M.P., Shen, Z., Törnqvist, T.E. and Mauz, B. (2017) Late Holocene evolution of a coupled, mud-dominated delta plain-chenier plain system, coastal Louisiana, USA. *Earth Surf. Dyn.*, **5**, 689–710.

Hori, K., Saito, Y., Zhao, Q. and Wang, P. (2002) Evolution of the coastal depositional Systems of the Changjiang (Yangtze) river in response to late Pleistocene-Holocene Sea-level changes. *J. Sediment. Res.*, **72**, 884–897.

ISOPT (1988) International symposium on penetration testing, 1988. Report of the ISSMFE technical committee on penetration testing. In: *Working Party*, Vol. **1**, pp. 27–51. ISOPT.

ISSMFE (1989) Appendix a: international reference test procedure for cone penetration test (CPT). In: *Report of the ISSMFE Technical Committee on Penetration Testing of Soils — TC 16, With Reference to Test Procedures*, Vol. **7**, pp. 6–16. Swedish Geotechnical Institute, Linköping.

Koster, K. (2016) Cone penetration testing: a sound method for urban archaeological prospection. *Archaeol. Prospect.*, **23**, 55–69.

Koster, K., Erkens, G. and Zwanenburg, C. (2016) A new soil mechanics approach to quantify and predict land subsidence by peat compression. *Geophys. Res. Lett.*, **43**, 10,792–10,799.

Koster, K., Stafleu, J., Cohen, K.M., Stouthamer, E., Busschers, F.S. and Middelkoop, H. (2018) Three-dimensional distribution of organic matter in coastal-deltaic peat: implications for subsidence and carbon dioxide emissions by human-induced peat oxidation. *Anthropocene*, **22**, 1–9.

Lafuerza, S., Canals, M., Casamor, J.L. and Devincenzi, J.M. (2005) Characterization of deltaic sediment bodies based on in situ CPT/CPTU profiles: a case study on the Llobregat delta plain, Barcelona, Spain. *Mar. Geol.*, **222–223**, 497–510.

Liu, J., Qiu, J., Saito, Y., Zhang, X., Nian, X., Wang, F., Xu, G., Xu, T. and Li, M. (2020) Formation of the Yangtze shoal in response to the post-glacial transgression of the paleo-Yangtze (Changjiang) estuary, China. *Mar. Geol.*, **423**, 106080.

Lo Presti, D., Meisina, C. and Squeglia, N. (2009) Applicabilità di prove penetrometriche statiche nella ricostruzione del profilo stratigrafico. *Riv. Ital. di Geotec.*, **2**, 9–33.

Long, M. and Donohue, S. (2010) Characterization of Norwegian marine clays with combined shear wave velocity and piezocone cone penetration test (CPTU) data. *Can. Geotech. J.*, **47**, 709–718.

Lorenzo, J.M., Hicks, J. and Vera, E.E. (2014) Integrated seismic and cone penetration test observations at a distressed earthen levee: Marrero, Louisiana, U.S.A. *Eng. Geol.*, **168**, 59–68.

Lunne, T., Robertson, P.K. and Powell, J.J.M. (1997) *Cone Penetration Testing in Geotechnical Practice*. EF Spon/ Blackie Academic, Routledge Publishers, London, 312 pp.

Maliva, R.G. (2016) *Aquifer Characterization Techniques*. Springer Hydrogeology, Berlin, 617 pp.

Miall, A.D. (2013) *The Geology of Fluvial Deposits: Sedimentary Facies, Basin Analysis, and Petroleum Geology*, 4th edn. Springer-Verlag, Berlin Heidelberg.

Missiaen, T., Verhegge, J., Heirman, K. and Crombé, P. (2015) Potential of cone penetrating testing for mapping deeply buried palaeolandscapes in the context of archaeological surveys in polder areas. *J. Archaeol. Sci.*, **55**, 174–187.

Monahan, P.A. (1999) *The Application of Cone Penetration Test Data to Facies Analysis of the Fraser River Delta*. University of Victoria, British Columbia.

Moran, K., Hill, P.R. and Blasco, S.M. (1989) Interpretation of piezocone penetrometer profiles in sediment from the Mackenzie trough, Canadian Beaufort Sea. *J. Sediment. Petrol.*, **59**, 88–97.

Muto, T. and Steel, R.J. (1997) Principles of regression and transgression: the nature of the interplay between accommodation and sediment supply. *J. Sediment. Res. Sect. B Stratigr. Glob. Stud.*, **67**, 994–1000.

Ori, G.G. (1993) Continental depositional systems of the quaternary of the Po plain (northern Italy). *Sediment. Geol.*, **83**, 1–14.

Pieri, M. and Groppi, G. (1981) *Subsurface Geological Structure of the Po Plain*. Verlag nicht ermittelbar, Liège.

Posamentier, H.W., Jervey, M.T. and Vail, P.R. (1988) Eustatic controls on clastic deposition I—conceptual framework. In: *Sea-Level Changes: An In- Tegrated Approach* (Eds Wilgus, C.K., Hastings, B.S., Kendal, C.G.C., Posamentier, H.W., Ross, C.A. and Van Wagoner, J.C.)*Special Publications of SEPM*, **42**, 109–124.

Powell, J.J.M. and Quarterman, R.S.T. (1995) Engineering geological mapping of soft clay using the piezocone. In: *Proc. Intl. Symp. on Cone Penetration Testing, CPT'95, Sweden*, Vol. **2**, pp. 263–268. Swedish Geotechnical Society.

Quinnan, J.A., Welty, N.R. and Killenbech, E. (2010) Hydrostratigraphic and permeability profiling for groundwater remediation projects. In: *2nd International Symposium on Cone Penetration Testing, Paper No. 3.33, Huntington Beach, California*. OmniPress, Madison, WI.

Rampello, S. and Callisto, L. (1998) A study on the subsoil of the tower of Pisa based on results from standard and high-quality samples. *Can. Geotech. J.*, **35**, 1074–1092.

Ricceri, G., Simonini, P. and Cola, S. (2002) Applicability of piezocone and dilatometer to characterize the soils of the Venice lagoon. *Geotech. Geol. Eng.*, **20**, 89–121.

Robertson, P.K. (1990) Soil classification using the cone penetration test. *Canadian Geotech. J.*, **27**, 151–158.

Robertson, P. (2010) Soil behaviour type from the CPT: an update. In: *2nd International Symposium on Cone Penetration Testing, CPT'10. Paper No. 2-56, Huntington Beach, California*. OmniPress, Madison, WI.

Robertson, P.K., Campanella, R.G., Gillespie, D. and Greig, J. (1986) *Use of Piezometer Cone Data, ASCE Speciality Conference In Situ '86: Use of In Situ Tests in Geotechnical Engineering*, pp. 1263–1280. American Society of Engineers (ASCE), Blacksburg.

Romeo, R., Amoroso, S., Facciorusso, J., Lenti, L., Madiai, C., Martino, S., Monaco, P., Rinaldis, D. and Totani, F. (2015) Engineering geology for society and territory – volume 5. In: *Urban Geology, Sustainable Planning and Landscape Exploitation* (Eds Lollino, G., Manconi, A., Guzzetti, F., Culshaw, M., Bobrowsky, P. and Luino, F.), pp. 1–1400. Springer International Publishing, Cham.

Salel, T., Bruneton, H. and Lefèvre, D. (2016) Ostracodes et variabilité environnementale dans les lagunes et deltas du nord-ouest de la Méditerranée (Golfe du Lion, France et delta de l'Ebre, Espagne). *Rev. Micropaleontol.*, **59**, 425–444.

Sarti, G., Rossi, V. and Amorosi, A. (2012) Influence of Holocene stratigraphic architecture on ground surface

settlements: a case study from the City of Pisa (Tuscany, Italy). *Sediment. Geol.*, **281**, 75–87.

Sarti, G., Rossi, V., Amorosi, A., Bini, M., Giacomelli, S., Pappalardo, M., Ribecai, C., Ribolini, A. and Sammartino, I. (2015) Climatic signature of two mid–late Holocene fluvial incisions formed under sea-level highstand conditions (Pisa coastal plain, NW Tuscany, Italy). *Palaeogeogr. Palaeoclimatol. Palaeoecol.*, **424**, 183–195.

Scarponi, D. and Angeletti, L. (2008) Integration of palaeontological patterns in the sequence stratigraphy paradigm: a case study from Holocene deposits of the Po plain (Italy). *GeoActa*, **7**, 1–13.

Schmertmann, J.H. (1969) *Dutch Friction-Cone Penetrometer Exploration of a Research Area at Field 5*. Eglin Air Force Base, Okaloosa, FL.

Schneider, J.A., Randolph, M.F., Mayne, P.W. and Ramsey, N.R. (2008) Analysis of factors influencing soil classification using normalized piezocone tip resistance and pore pressure parameters. *J. Geotech. Geoenvironment Eng.*, **134**, 1569–1586.

Schokker, J. and Koster, E.A. (2004) Sedimentology and facies distribution of Pleistocene cold-climate aeolian and fluvial deposits in the Roer Valley graben (southeastern Netherlands). *Permafr. Periglac. Process.*, **15**, 1–20.

Schoustra, J.J. (1975) Application of static cone penetrometer tests for determining continuity of stratigraphic horizons. In: *Proceedings of the European Symposium on Penetration Testing ESOPT, Stockholm, June 5–7, 1974, 2:1 General Reports, Discussions and Other Activities*, pp. 150–154. National Swedish Building Research.

Schwarz, E., Veiga, G.D., Spalletti, L.A. and Massaferro, J.L. (2011) The transgressive infill of an inherited-valley system: the Springhill formation (lower cretaceous) in southern Austral Basin, Argentina. *Mar. Pet. Geol.*, **28**, 1218–1241.

Shanley, K.W. and McCabe, P.J. (1991) Predicting facies architecture through sequence stratigraphy - an example from the Kaiparowits plateau, Utah. *Geology*, **19**, 742–745.

Soil Survey Staff (1999) *Soil Taxonomy: A Basic System of Soil Classification for Making and Interpreting Soil Surveys*, 2nd edn. Natural Resources Conservation Service, USDA, Washington, DC, 886 pp.

Stegmann, S., Sultan, N., Kopf, A., Apprioual, R. and Pelleau, P. (2011) Hydrogeology and its effect on slope stability along the coastal aquifer of Nice, France. *Mar. Geol.*, **280**, 168–181.

Storms, J.E.A., Weltje, G.J., Terra, G.J., Cattaneo, A. and Trincardi, F. (2008) Coastal dynamics under conditions of rapid sea-level rise: late Pleistocene to early Holocene evolution of barrier-lagoon systems on the northern Adriatic shelf (Italy). *Quat. Sci. Rev.*, **27**, 1107–1123.

Styllas, M. (2014) A simple approach to define Holocene sequence stratigraphy using borehole and cone penetration test data. *Sedimentology*, **61**, 444–460.

Swift, D.J.P. (1968) Coastal erosion and transgressive stratigraphy. *J. Geol.*, **76**, 444–456.

Tanabe, S., Saito, Y., Lan, V.Q., Hanebuth, T.J.J., Lan Ngo, Q. and Kitamura, A. (2006) Holocene evolution of the song Hong (Red River) delta system, northern Vietnam. *Sediment. Geol.*, **187**, 29–61.

Tanabe, S., Nakanishi, T., Matsushima, H. and Hong, W. (2013) Sediment accumulation patterns in a tectonically subsiding incised valley: insight from the Echigo plain, Central Japan. *Mar. Geol.*, **336**, 33–43.

Tanabe, S., Nakanishi, T., Ishihara, Y. and Nakashima, R. (2015) Millennial-scale stratigraphy of a tide-dominated incised valley during the last 14 kyr: spatial and quantitative reconstruction in the Tokyo lowland, Central Japan. *Sedimentology*, **62**, 1837–1872.

Taylor, B.B., Lewis, J.F. and Ingersoll, R.W. (1993) Comparison of interpreted seismic profiles to geotechnical borehole data at Hibernia. In: *Proceedings of the Fourth Canadian Conference on Marine Geotechnical Engineering*, St. John's, Newfoundland, June 27–30, pp. 684–708.

Teatini, P., Tosi, L. and Strozzi, T. (2011) Quantitative evidence that compaction of Holocene sediments drives the present land subsidence of the Po Delta, Italy. *J. Geophys. Res. Solid Earth*, **116**, 1–10.

Törnqvist, T.E., Wallinga, J., Murray, A.S., De Wolf, H., Cleveringa, P. and De Gans, W. (2000) Response of the Rhine-Meuse system (west-Central Netherlands) to the last quaternary glacio-eustatic cycles: a first assessment. *Glob. Planet. Change*, **27**, 89–111.

Törnqvist, T.E., Wallace, D.J., Storms, J.E.A., Wallinga, J., Van Dam, R.L., Blaauw, M., Derksen, M.S., Klerks, C.J.W., Meijneken, C. and Snijders, E.M.A. (2008) Mississippi Delta subsidence primarily caused by compaction of Holocene strata. *Nat. Geosci.*, **1**, 173–176.

Truong, M.H., Nguyen, V.L., Ta, T.K.O. and Takemura, J. (2011) Changes in late Pleistocene-Holocene sedimentary facies of the Mekong River Delta and the influence of sedimentary environment on geotechnical engineering properties. *Eng. Geol.*, **122**, 146–159.

Truong, H.M., Van Nguyen, L., Ta, O.T.K. and Takemura, J. (2013) The late Pleistocene-Holocene sedimentary facies and geotechnical properties of CLM1 core at Cao Lanh city Mekong river delta. *Sci. Technol. Dev. J.*, **16**, 29–37.

Truong, M.H., Nguyen, L., Ta, T.K.O. and Takemura, J. (2016) The influence of delta formation mechanism on geotechnical property sequence of the late Pleistocene-Holocene sediments in the Mekong River Delta. *Heliyon*, **2**, 1–40. https://doi.org/10.1016/j.heliyon.2016.e00165.

Van Wagoner, J.C., Mitchum, R.M., Campion, K.M. and Rahmanian, V.D. (1990) Siliciclastic sequence stratigraphy in well logs, cores, and outcrops: concepts for high-resolution correlation of time and facies. *AAPG Methods Explor.*, **7**, 55.

Vannoli, P., Burrato, P. and Valensise, G. (2015) The Seismotectonics of the Po plain (northern Italy): tectonic diversity in a blind faulting domain. *Pure Appl. Geophys.*, **172**, 1105–1142.

Vos, P.C., Bunnik, F.P.M., Cohen, K.M. and Cremer, H. (2015) A staged geogenetic approach to underwater archaeological prospection in the port of Rotterdam (Yangtzehaven, Maasvlakte, The Netherlands): a geological and palaeoenvironmental case study for local mapping of Mesolithic lowland landscapes. *Quat. Int.*, **367**, 4–31.

Watts, B.D., Seyers, W.C. and Stewart, R.A. (1992) *Liquefaction Susceptibility of Greater Vancouver Area Soils Geotechnique and Natural Hazards*, pp. 145–157. BiTech Publishers, Vancouver, BC.

Zhang, X., Lin, C.M., Dalrymple, R.W., Gao, S. and Li, Y.L. (2014) Facies architecture and depositional model of a macrotidal incised-valley succession (Qiantang River estuary, eastern China), and differences from other macrotidal systems. *Bull. Geol. Soc. Am.*, **126**, 499–522.

Zhang, X., Lin, C.M., Dalrymple, R.W., Gao, S. and Canas, D.T. (2018) Use of the cone penetration testing (CPT)

method to interpret late quaternary tide-dominated successions: a case study from the eastern China coastal plain. *Cont. Shelf Res.*, **161**, 49–57.

Zhang, X., **Lin, C.M.**, **Dalrymple, R.W.** and **Yang, S.Y.** (2021) Source-to-sink analysis for the mud and sand in the late-quaternary Qiantang River incised-valley fill and its implications for delta-shelf-estuary dispersal systems globally. *Sedimentology*, **68**, 3228–3252.

Zoccarato, C., **Minderhoud, P.S.J.** and **Teatini, P.** (2018) The role of sedimentation and natural compaction in a prograding delta: insights from the mega Mekong delta, Vietnam. *Sci Rep.*, **8**, 11437.

Zoccarato, C., **Törnqvist, T.E.**, **Teatini, P.** and **Bridgeman, J.G.** (2020) A shallow compaction model for Holocene Mississippi Delta sediments. *Proc. Int. Assoc. Hydrol. Sci.*, **382**, 565–570.